NASA TECHNICAL MEMORANDUM

NASA TM-77740

DFVLR ROTORCRAFT-- CONSTRUCTION AND ENGINEERING

H.J. Langer

Translation of "DFVLR-Rotorversuchsstand-- Konstruktion und Entwicklung," Deutsche Forschungs und Versuchsanstalt fuer Luft- und Raumfahrt, Institut fuer Flugmechanik, Braunschweig, West Germany, Report, (1984?) pp. 1-60.

NATIONAL AERONAUTICS AND SPACE ADMINISTRATION
WASHINGTON D.C. 20546 AUGUST 1984

31 1 1 RN/NASA-TM-77740
DISPLAY 31/2/1
85N10035*# ISSUE 1 PAGE 6 CATEGORY 5 RPT#: NASA-TM-77740 NAS
1.15:77740 CNT#: NASW-3542 84/08/00 64 PAGES UNCLASSIFIED DOCUMENT
UTTL: DFVLR rotorcraft: Construction and engineering
AUTH: A/LANGER, H. J.
CORP: National Aeronautics and Space Administration, Washington, D.C.
AVAIL.NTIS
SAP: HC A04/MF A01
COI: UNITED STATES Transl. by Scientific Translation Service, Santa Barbara, Calif. Original doc. prep. by Inst. fuer Flugmechanik, DFVLR, Brunswick Transl. into ENGLISH of ""DFVLR-rotorversuchsstand-konstruktion und entwicklung'' rept. Brunswick, 1984 60 p
MAJS: /*AERODYNAMIC CONFIGURATIONS/*HELICOPTER DESIGN/*HELICOPTER PERFORMANCE/* ROTARY WINGS/*TEST STANDS/*WIND TUNNEL TESTS
MINS: / ACTUATORS/ DYNAMIC STRUCTURAL ANALYSIS/ HYDRAULIC EQUIPMENT/ MANUFACTURING/ STATIC STABILITY/ WIND TUNNELS
ABA: M.A.C.
ABS: A helicopter rotor test stand is described. Full scale helicopter components can be tested such as hingeless fiberglass rotors and two blade rotor with flapping hinge, or a hybrid system. The facility is used to test stability, rotor components and downwind components.

ENTER:
DISPLAY 31/2/1
85N10035*# ISSUE 1 PAGE 6 CATEGORY 5 RPT#: NASA-TM-77740 NAS
1.15:77740 CNT#: NASW-3542 84/08/00 64 PAGES UNCLASSIFIED DOCUMENT
UTTL: DFVLR rotorcraft: Construction and engineering
AUTH: A/LANGER, H. J.
CORP: National Aeronautics and Space Administration, Washington, D.C.
AVAIL.NTIS
SAP: HC A04/MF A01
COI: UNITED STATES Transl. by Scientific Translation Service, Santa Barbara, Calif. Original doc. prep. by Inst. fuer Flugmechanik, DFVLR, Brunswick Transl. into ENGLISH of ""DFVLR-rotorversuchsstand-konstruktion und entwicklung'' rept. Brunswick, 1984 60 p
MAJS: /*AERODYNAMIC CONFIGURATIONS/*HELICOPTER DESIGN/*HELICOPTER PERFORMANCE/* ROTARY WINGS/*TEST STANDS/*WIND TUNNEL TESTS
MINS: / ACTUATORS/ DYNAMIC STRUCTURAL ANALYSIS/ HYDRAULIC EQUIPMENT/ MANUFACTURING/ STATIC STABILITY/ WIND TUNNELS
ABA: M.A.C.
ABS: A helicopter rotor test stand is described. Full scale helicopter components can be tested such as hingeless fiberglass rotors and two blade rotor with flapping hinge, or a hybrid system. The facility is used to test stability, rotor components and downwind components.

ENTER:

STANDARD TITLE PAGE

1. Report No. NASA TM-77740	2. Government Accession No.	3. Recipient's Catalog No.
4. Title and Subtitle DFVLR ROTORCRAFT-- CONSTRUCTION AND ENGINEERING		5. Report Date AUGUST 1984 6. Performing Organization Code
7. Author(s) H.J. Langer		8. Performing Organization Report No. 10. Work Unit No.
9. Performing Organization Name and Address SCITRAN Box 5456 Santa Barbara, CA 93108		11. Contract or Grant No. NASw- 3542 13. Type of Report and Period Covered Translation
12. Sponsoring Agency Name and Address National Aeronautics and Space Administration Washington, D.C. 20546		14. Sponsoring Agency Code

15. Supplementary Notes

Translation of "DFVLR-Rotorversuchsstand-- Konstruktion und Entwicklung," Deutsche Forschungs und Versuchsanstalt fuer Luft- und Raumfahrt, Institut fuer Flugmechanik, Braunschweig, West Germany, Report, (1984?) pp. 1-60.

16. Abstract

A helicopter rotor test stand for the DFVLR is described. Full scale helicopter components can be tested: hingeless fiberglass rotors and 2-blade rotor with flapping hinge, or a hybrid system. The facility is used to test stability, rotor components and downwind components.

17. Key Words (Selected by Author(s))	18. Distribution Statement Unclassified and Unlimited		
19. Security Classif. (of this report) Unclassified	20. Security Classif. (of this page) Unclassified	21. No. of Pages 64	22. Price

Table of Contents /2*

---

*Numbers in the margin indicate foreign pagination.

DFVLR Rotor Test Stand - Design and Development /3

Introduction

The development of helicopters presently manufactured on an assembly line has reached its limits in terms of flight performance (speed, range).

Further developments require better knowledge of the fundamentals, the control of conventional methods, and the development of possibilities for improving conventional systems. In order to improve performance, it is very important to investigate new kinds of configurations based on a modern rotor concept.

Extensive wind tunnel tests are required to complement and verify theoretical analysis. Therefore the following tests were planned in the wind tunnel during the intial phase:

- Investigation of the static stability behavior of the rotor
- Measurement of dynamic rotor components
- Downwind measurements.

Since already in the definition phase it was clear that performance improvements in helicopters could be brought about by influencing the blade aerodynamics, we decided to use two principally different rotor systems.

- A hingeless GfK (fiberglass reinforced plastic) rotor as a model of the BO 105 with shaft drive (hingeless rotor)
- a 2-blade rotor with a central flapping hinge (teetering rotor), which can be used both by using reaction drive and shaft drive, as well as the combination of the two drive systems (hybrid).

The results are of interest in such investigations by industry. We found that at the request of the DFVLR, a rotor test stand for large wind tunnels was to be built. It has to be capable of satisfying the various requirements from project oriented research and basic research. /4

In the design of the test facility we assumed that a wind tunnel was only required for producing the drive wind. Otherwise, the system had to be completely independent except for electrical power supply.

1. Rotor Carriers

In the definition of the tasks when building up the rotor test stand, the DFVLR was given the task of designing and manufacturing the rotor carrier (Fig. 1).

1.1 Drive System

1.1.1 Hydraulic Pump

A hydraulic facility was used as a drive system, which is driven by an electrical motor (Fig. 2). The hydraulic installation essentially consists of two parts: a hydropump and a hydromotor. Both are connected through hose lines over 11 meters long. The separation of the hydromotor and the hydropump has the advantage that the rotor carrier itself can be designed in a relatively narrow way. The hydromotor has a power of about 90 kW at 1050 rpm.

The hoses are connected to the test stand using fast disconnect couplings. This has the advantage that connections can be made without tools and very fast. Anti-return valves make it unnecessary to remove air from the hydraulic system.

In order to simplify the installation and increase operational safety, all of the additional equipment required for a closed circuit with a supply unit are enclosed in tubes. This includes supply valves, rinsing valves and supply pressure valves, safety valves, auxiliary pumps, air coolers, filters and pumps (Fig. 3). Because of the total length of the hoses (< 30 m outgoing and return line) an additional oil switch is not necessary. The auxiliary pump provides a continuous fluid flow through filters and air oil coolers for compensating leakages, cooling and liquid exchange in the main circuit. The excess fluid produced by the supply system is removed from the main circuit through a rinsing and supply pressure valve, from the low pressure side. /5

The drive current of the primary part is proportional to the drive. By turning on the adjustment motor, the supply volume can be changed continuously using a reduction gear and a self-retarding threaded spindle. The running of the hydromotor in the left and right directions is adjusted here. For safety reasons, the end positions are mechanically fixed. Since we are using supply operation, supply occurs in the opposite direction, when one passes through the zero position.

1.1.2 Hydraulic Motor

An axial piston motor using a oscillating drum design with a constant lift volume per revolution is used as a rotor drive system. The principle of the motor is given in Fig. 4. The liquid is pressed into one side of a cylinder by the valve plate, and this forces the piston in the side of the cylinder away from the plate. The force of the piston rotates the axis, because the cylinder block is inclined with respect to the axis drive.

The swallowing current is proportional to the rpm and the torque being delivered increases with the pressure difference between the high pressure side and the low pressure side (Fig. 5).

When selecting the hydraulic liquid, it is important to realize that it is not only used for energy transmission but also has a lubrication function. Therefore, a liquid /6 has to be used with good adhesion properties and wear properties. This is required so that the required pressures and rotation rates can be adjusted.

The drive unit was selected so that the maximum torque load is around 930 Nm and corresponds to a pressure of a maximum of 275 bar. Pressure peaks up to 400 bar are allowed.

1.1.3 Hydraulic Tipping Facility (Fig. 6)

The hydraulic tipping facility is installed on the fixed column between the fixed and moveable part. The hydraulic cylinder is installed outside the fixed part, as is the installation plate with the various valves, etc. By using a hydraulic double lock, it is possible to lock the tipping device. This means that a static rotor angle of attack can be maintained over a long period. The velocity with which the tipping device can be adjusted in the positive and negative directions is adjusted at two-path flow control valves. From a 40 liter tank, the hydraulic oil is pressed into a hydraulic storage unit using a cog wheel pump (Q = 2,7 l/min, P = 120bar.) which is driven by an electrical motor (N = 750 W). The system pressure is maintained between 100 bar and 120 bar by two pressure signaling devices. If the required pressure is present, then the hydraulic cylinder is

controlled through a electromagnetic valve. The cylinder has an adjustment path which corresponds to a rotor angle of attack range of $-17^{\circ} \leq \alpha_{Ro} \leq +15^{\circ}$.

We did not consider free motion between the rotor shaft and the hydraulic motor connected with a coupling-braking combination as originally planned. This is because the heat development during the braking process was undesirable. Also the lamella coupling generated imbalances in the fixed column.

1.2 Balance Systems

The rotor test stand was equipped with two balances, in order to measure forces and moments over the fuselage and on the rotor head.

One design difficulty consisted of the fact that the required rotor power has to be transferred through the balance to the rotor shaft without falsifying the measurement points.

1.2.1 Rotor Balance

Since the balance will be discussed in detail in the chapter on "Measurement Data Collection," we will only give a short description of its design.

The rotor balance consists of a lower plate on which there are installed seven force measurement capsules, and the upper plate where the transmission elements are installed. There is a torque measurement shaft between two lamella packages between the upper and lower plates. These lamella packages ensure that only the rotor torque is transmitted and tipping moments only are recorded by the balance. The

forces in the longitudinal direction, transverse direction and thrust direction are also only transmitted to the balance. This means that the balance is independent of the influences of the drive. The requirement of having the least possible distance between the rotor plane and the measurement plane of course can only be maintained within certain limits, because control of the rotor has to be maintained. The smaller the design height, the lower will be the lever arms and therefore the forces on the force measurement capsules. Fig. 7 shows the balance control configuration in an old version. In a newer version, the measurement plane is placed higher up because of the better geometric conditions, in the direction of the upper plane. Later on we will discuss that there are some problems associated with this configuration.

The transmission elements from the force measurement capsule /8
to the upper plate on the one hand should be as elastic as possible so that the force measurement capsule does not have to absorb any transverse forces. On the other hand, it should be as rigid as possible, so that the oscillation system consisting of the lower balance part and the upper balance part (plate, control, rotor and telemetry) has the highest possible eigen frequencies.

The transmission elements consist of steel wires 4 mm in diameter in the x, y direction and the z direction. These wires are pasted onto the corresponding sensors. We found that the glue did not have the required continuous strength, because it became separated from the transmission elements which we barely noticed. This "creeping effect" is only found when the balance is calibrated again, which would occur before and after each test run. Also, we made our own investigations of whether the measurement capsule signals return to the original values.

The transmission elements which were used today are rotating parts made of copper-beryllium with completed connection pieces for the force measurement capsules and for the upper holders. This material can be worked easily and has good stiffness values.

For safety reasons, the balance can be electromagnetically locked by two bolts, so that horizontal oscillations such as occur when the rotor is raised do not affect the force measurement capsules. As soon as the rotor has reached a specified rotation rate, the balance is released. Also, there are supports between the balance plates which hold the upper plate and lower plate system in a centered fashion when the balance is overloaded. When designing the balance we have to ensure that the system will be as stiff as possible, so that a twisting of the upper plate or a bending of the support arms is prevented. This has the advantage that, when calibrating the system, terms of higher order can be ignored. /9

1.2.2 Fuselage Balance

The fuselage balance based on DMS (strain gauges) also had seven force measurement capsules just like the rotor balance. One DMS balance will only provide useable results if the balance reference point is as close as possible to the force application point of the model. In order to be able to satisfy this condition, we selected a box balance which is elongated in all directions, which was built up around the rotor shaft. In the case of the model fuselage matched to this balance, the balance is below the fuselage and has to be covered with a covering body against the wind tunnel flow.

The DMS balance essentially consists of two steel plates which are stiff with respect to bending, between which the

measurement capsules and the holders as well as the soft bending rods are arranged as transmission elements. The lower steel plate of the balance is connected to the model and with the model fuselage through consoles.

In order to calibrate the balance, a calibration frame and a force introduction frame had to be built. With these frames, the three forces and the three moments were introduced according to a certain calibration scheme (Fig. 8). The calibration determines the following three parameters:

1. Direct calibration factors which can be derived from geometric dimensions.

2. Linear interference factors, which result from the fact that the system is not completely uncoupled. This means, for example, force in the x-direction gives a signal in the z-capsule.

3. Product interferences which result when two components act on a force mesurement capsule. For example, force in the x-direction and the y-direction results in a signal in the z-capsule.

As the calibration matrices show, the values due to product interferences are small. This is because of the fact that the elastic deformations are small for the loads which occur. /10

1.3 Control

Three actuation motors attached to the upper plate, the swash plate and the rotating control rods which deflect the blades make up the rotor control system.

1.3.1 Blade Control

The conversion of the actuation paths from the aircraft-fixed system into the rotating system is done through the swash plate (Fig. 9). By a translation motion in the z-direction and a rotation around the longitudinal axis and the transverse axis, it makes the blades move collectively and cyclically.

The transmission of the actuation paths to the blade has to be done so that the desired amplitude variation occurs in the blade, both in terms of magnitude and phase.

Usually one defines three control angles on a rotor: collective angle, longitudinal control angle and transverse angle. The total angle at the blade is derived from the following relationship:

$$\theta_{Blade} = \vartheta_o + \theta_s \sin\psi + \theta_c \cos\psi \ .$$

In the case of completely controlled flights, θ_s is always negative and ϑ_c is always positive, where it is assumed that the rotor rotates in a counter-clockwise fashion. The blade angle is the smallest for $\psi = 90^\circ$, for purely longitudinal control and for $\psi = 0^\circ$ it is largest for the pure transverse control angle. In order to produce a pure pitching moment on the rotor it is not sufficient to only operate the longitudinal control unit. Instead, a transverse control deflection has to be implemented. This task is called phase shift and is only /11 dependent on the flapping hinge distance, if one assumes that the aerodynamic damping is the same for all of the rotors. A rotor with a central flapping hinge therefore has a phase shift of 90° and a propeller has a shift of 0°. For the research rotor, it is about 80°. This has to be taken into consideration if the rotor has to be controlled according

to flight characteristics. That is where longitudinal control input results in a pitching moment.

The control was dimensioned in such a way, that the reaction rotor mentioned at the beginning which requires a large shaft diameter for passing through gas can be operated. This requires a larger swash plate and a modified control kinematics. The conversion of the actuation paths from the electrical motors to the blade angle variation is done through an analog computer.

One disadvantage is that the relationship between the actuation path and the blade angle cannot be linearized. When designing the swash plate, one should design the geometric parameters of the rotor blade in such a way that the trigonometric functions can be linearized. If this is not possible, the analog computer circuit becomes rather complicated because of the required SIN and COS function components. Fig. 10 gives a diagram of the geometric relationship between the actuation paths z_1, z_2, and z_3 and the blade angle ($\vartheta_o \equiv \vartheta_{blade}$).

The following data are important for designing the control system:

Blade number	z = 4 m
Rotor rpm	n = 1050 rpm
Required path of the swash plate (for collective control)	s = ±9.6 [mm]
Required inclination angle of the swash plate (for cyclical control)	$\alpha = \pm 10{,}5^{\circ}$

/12

We use the following loads in the calculations. These only occur at extreme operational conditions.

Axial force	400 [N] $\pm$ 60 [N]
Tipping moment, longitudinal	7 [N] $\pm$ 3 [Nm]
Tipping moment, transverse	11,5 [Nm] $\pm$ 9 [Nm]
Resulting force at an actuator deflection point	P_{max} 320 [N]

In order to have universal applicability in other rotors, the control should have reserves with respect to these data. For instance, the axial path can be raised to -12/+15 [mm], the inclination can be raised to $\alpha_{max} = \pm 14^{\circ}$ and the permissible force per actuator could be raised to $P_{zul} = 480$ [N].

It has been found that in many test configurations the permissible actuator force can even be exceeded.

The swash plate is structured as follows from the inside to the outside (Fig. 11). The basic element is a flange cover made of stainless steel, part No. 9, whose inner diameter is such that both the mechanical rotor shaft and the exchange of the rotor mass which carries air can be passed through it. There is a spherical ring, part No. 3, on the cover, which is installed so it can be displaced in height in order to allow collective control. Because of the good sliding properties, aluminium-bronze was used as a material for the spherical ring. The fixed part of the swash plate can be rotated on the sphere (for cyclical control). The lower part 1 and the upper part 2 are connected with bolts, and on the inside they enclose the spherical ring with their rounded sliding surfaces. On the outside they also hold the inner ring of the 4-point bearing.

In order to prevent rotation of the fixed part of the swash plate, it is held through two columns which move in curved grooves and they are held radially on the spherical ring. It is supported by two pass springs on the flange cover. There are three fork shaped openings nailed into this separated by 120°, in which the thrust rods of the three actuation motors are supported by jointed bearings which require no maintenance. The rotating parts of the swash plate, parts 7 and 8, are tensioned by the outer ring of the 4-point bearing. Both parts have labyrinth like grooves, in order to seal off the inner part of the bearing which is filled with grease. This is propelled in the direction of rotation by the rotor head through a scissors having a hinged bearing. There are four cavities into which the hinged bearings of the control rods penetrate. /13

1.3.2 Swash Plate Control with Electrical Actuators

Three actuation motors are required for controlling the swash plate. The actuators must have the greatest possible paths so that the complete possibilities of lifting and tipping of the swash plate can be exploited. In order to obtain the simplest possible control loop, linear motors are used. One of the difficulties is that the torsion moments have to be compensated for by the rotor blade if such a large actuation force is to be produced with such a small size. It was determined that a maximum actuation force of 450 N was sufficient.

The following are the technical details:

Design:	Linear actuator
Current type and voltage	= 28 [V]

Current supply (maximum)	about 2 [A]
Actuation rate at a load of 450 [N]	2.8 [mm/s]
Lift	64 [mm], can be expanded to 85 [mm]
Lift limit	With end switch
Actuator force per actuator	450 [N]
Gear	Self-retarding
Actual lift value	Potentiometer
Resistance of the potis (potentiometer)	1 [kΩ]

/14

Investigations have shown that the running rate of the actuators is almost the same. Therefore, it is not possible for cyclical angles to be given to the rotor when there are collective changes.

In order to maintain the deviation between the nominal value and the actual value of the control angles to be adjusted, the actuation motors have an additional brake in order to prevent overshoot. Potentiometers are used to relay back the nominal value.

1.3.3 Swash Plate with Hydraulic Actuators

Compared with electrical actuators, hydraulic actuators have two special advantages. 1. Large loads can be overcome with relatively small actuators. 2. Diameter control signals can be better transmitted. The running of pressure lines and the hydraulic supply are a disadvantage because they are complex. Also, the electrical actuators are much cheaper than hydraulic actuators, because of the small cost of the periphery.

The decision of replacing the electrical actuators by electro-hydraulic actuators was influenced essentially by additional research work in the area of active control. The possibility of inputting dynamic control signals into the swash plate opens up a large area of research on which much work is now in progress. Essentially there are three applications, which could be investigated with this method:

- Reduction of rotor-induced vibrations in the range between $3\ \Omega_{RO}$ to $5\ \Omega_{RO}$. /15
- Gust reduction
- Determination of dynamic derivatives.

At the present time for the model rotor we are only investigating the area of reducing rotor-induced vibrations, which we will report on in a future paper.

The requirements for the actuator motors are the greatest for the tasks of reducing vibrations, because trigonometric functions have to be input up to the limiting frequency of 80 Hz.

The following specifications were established (Fig. 12):

Design height	$\leq$ 233 mm $\pm$ 32 mm
Displacement path	$\pm$ 32 mm
Load	500 N $\pm$ 300 N dynamics
Mass forces	$\leq$ 3 kg
Actuator frequencies	80 Hz at $\pm$ 3 mm lift
For SIN operation	20 Hz at $\pm$ 7 mm lift

In the calculations for the design of the actuator, we assumed a system pressure of 210 bar*. This pressure has to be available to the servo valves as supply pressure. Therefore the flow losses

* 1 bar = 10^5

in the 15 meter long lines have to be made as small as possible, that is, only really necessary fast connection parts may be used and the line has to be bent as little as possible. The return line pressure also has to be made small. This can be done by a large dimension line diameter, which does not have any influence on the dynamic behavior of the drives.

In order to obtain a constant pressure as much as possible, a pressure reservoir is installed ahead of the servo valves. In the return line, that is, after the actuator drives, there is a reservoir with a low preliminary voltage (4 bar). This is to prevent diesel and cavitation effects which are caused by long return lines. An anti-return valve in the return line makes sure that the oil column does not break up. /16

In order to ensure certain operation and so that the transmission behavior of the actuator remains constant, the degree of contamination of the hydraulic liquid is an important factor. Therefore, in the initial line, filters with contamination indications are installed. The filter fineness is 3 µm (10^{-6}m) with a nominal flux of 80 l/min.

In order to not obtain any dangerous load states on the rotor in the case where there is a failure of the hydraulic supply or if the electrical control system of the actuator fails, so-called fail safe manifolds (fast-operating blocking valves) are installed, which prevent the actuator from reaching the hard stop position (end position).

The electrohydraulic actuators consist of the following:

a) Servo cylinder with 4-edge design, loaded twice (uniform motion cylinder) with piston rod on one side. Test pressure: 360 bar; maximum piston velocity: 90 m/min; piston diameter: 25 mm; piston rod diameter: 14 mm.

b) Path indicator, installed on the side with a linearity of 0.3% of the total traveled.

c) Blocking valve, fast acting.

d) High response servo valve with a nominal flux of 38 1/min for a valve pressure drop of 70 bar. Continuous operating pressure: 210 bar (Fig. 13).

This figure shows the design of a servo valve. The torque motor with the spring and the control piston is the central part of this valve. The edges of the control piston and the edges in the surrounding cylinder are especially subject to wear. Therefore, any deviation from the nominal dimensions is then felt by a corresponding error in the transmission function. Since we /17
cannot assume that all actuators are equipped with servo valves having no tolerances, they therefore also have different transmission functions. As I already mentioned, contamination in the control edges of the pistons has a great influence on the dynamic behavior of the servo.

The rough calculations made during the design about the dynamic actuator behavior for an amplitude height of ±3 mm, could not be realized in practice. The reason for this is the deficient knowledge about the entire control path. Therefore, it was not possible to take into account the nonlinear influences such as the coulomb friction of the cylinder and that of the bearings as well as the spring stiffness and damping characteristics of the coupled components, which is necessary for an exact calculation.

The design goals, that is

90° phase displacement at about 75 Hz
45° phase displacement at about 35 Hz
100% amplitude at about 80 Hz

were not achieved as Fig. 14a and Fig. 14b show. The actual values are the following

90° phase displacement at 32 Hz
45° phase displacement at 16 Hz
100% amplitude at 50 Hz

However, the required values can be obtained without difficulty by means of an adjustment. An adjustment is necessary because the frequency and phase variation of the actuators depend on the following

a) The zero position of the actuator piston
b) The load on the actuator
c) The amplitude around the working point
d) The dynamic behavior of the high-response servo
e) The degree of contamination.

One suggestion for implementing the designed actuator behavior is shown in Fig. 15. Each actuator is equipped with such a controller, in order to obtain the same actuator characteristics. The principle consists of controlling these phases as well as the magnitude in such a way until the deviation from a reference curve has become zero. Results from tests with and without the controller are shown in Fig. 16. It can be seen that amplitude and phase positions can be maintained constant over the considered frequency range. /18

2. Rotor and Fuselage

When designing a model rotor or a model fuselage, the application is very important. The question of which research task is to be investigated with the model first has to be answered. Fundamental research can only be

performed conditionally with a model that does not allow any modifications. On the other hand, such a model can be used very efficiently to test the correlation between measurements and calculations.

A model derived from a full scale version in addition has the possibility of correlating measurement results from flight tests and wind tunnel tests with calculations.

After agreement was reached with the customers, two rotor models and one fuselage model were constructed and manufactured. The important data follow:

Research Rotor I (Fig. 17)

Design:	hingeless, shaft drive
Diameter:	D = 4 m
Number of blades:	n = 4
Area density:	$\sigma_{0,7} = 7{,}64$ %
Blade shape:	rectangular; -8°/m linear twist
Blade profile:	NACA 23012
Blade tip velocity:	U_{Tip} = 220 m/s /19
Flapping frequency ratio:	$\omega_{\beta}/\Omega = 1{,}12$
Deflection frequency ratio:	$\omega_{\zeta}/\Omega = 0{,}71$
Design thrust:	T = 3600 N
Maximum thrust for hovering flight:	T_{max} = 4400 N
Lock coefficient:	4.47
Blade material:	GfK (fiber reinforced plastic) with foam, core and lead center
Rotor head material:	Steel
Manufacturer:	MBB

Research Rotor II (Fig. 18)

Design:	2-blade rotor with central flapping hinge, reaction - and/or shaft drive
Diameter:	D = 4 m
Blade number:	n = 2
Area density:	$\sigma_{0,7}$=6,05 %
Blade shape:	Rectangle; -5°/m linear twist
Cone angle:	β_o = 0° 54'
Blade profile:	NACA 63_3 -013
Blade tip velocity:	220 m/s
Flapping frequency ratio:	ω_β/Ω= 1,09
Deflection frequency ratio:	ω_ζ/Ω= 1,13
Deflection thrust:	T = 3600 N
Lock:	5.095
Blade material:	Aluminum, strand cast profile for conducting gas, Al honeycomb
Rotor head material:	Steel
Manufacturer:	Dornier/DFVLR

Fuselage /20

Length:	3.85 m
Width:	0.66 m
Height:	0.55 m
Material:	GfK shell (glass fiber reinforced plastic), Al (aluminum) frame
Manufacturer:	MBB (previously VFW-Fokker)

Since most of the results are available from tests with the research rotor I, we will now discuss the design and manufacture of the 4-blade rotor because this rotor belongs to one of the most modern designs because of its construction.

2.1 Specification of the Main Data of the Rotor Blades

In order to provide enough margin on operating strength and a freedom from ground resonance of the model rotor, it is designed as much as possible with dynamic similarity with respect to the main rotor of the BO 105. The linear reduction scale therefore is to be s = 2.5 (s-scale factor). The rotor blade for hingeless rotors has an important effect on whether dynamic similarity with the BO 105 blade has been achieved because of its elastic characteristics and its mass distribution. Therefore, maintaining the specified stiffness distributions and mass distributions is an important part of the design. Compared with the rotor blade of the main design, the linear reduction of all lengths and wall thicknesses is carried out, with some exceptions, and the same blade design made of GfK is used (glass fiber reinforced plastic) in order to obtain the closest possible material values.

2.1.1 Blade Chord

In order to have dynamically similar aerodynamic forces which act on the rotor blade, the blade tip velocity of the rotor blades is made equal to that of the full-scale version. For /21
this purpose the rotation rate of the model rotor has to be increased 2.5 times. By using the same blade profile the Mach numbers are provided for. Since the Re number in the case of Mach number similarity cannot be maintained, the blade chord is made slightly larger than for linear scaling. In the case of rotor blades, the fact that the same Re number is not insured is not so serious as for a lifting wing. Therefore, in the case of the model rotor, when there was linear reduction, the aerodynamic forces relative to the mass forces and elastic forces became too small. Therefore, it was appropriate to make the blade chord somewhat greater, that is, c = 0.121 m.

2.1.2 Cross-sections for Maintaining the Frequency Ratios

In the case of helicopters and also during rotor test stand tests, ground resonance is influenced by the deflection frequency ratio of the rotor and the magnitude of its deflection damping. In the large version, a frequency ratio of $\omega_\zeta/\Omega = 0{,}666$ and 2% to 3% of the critical damping are sufficient in order to exclude ground resonance. When there is geometric reduction, it is not certain that the parts which are important for damping, such as for example the grommet, the blade covering and the blade throat will result in a dynamically similar damping coefficient, the frequency ratio is increased to $\omega_\zeta/\Omega > 0{,}7$ in the case of the model rotor blade. Therefore it is possible to exclude the possibility of ground resonance when the damping reduces to $< 2\%$ of the critical damping of the rotor. The rotor blades therefore have to be stiffer at the blade root in the case of the model in the deflection direction. This is achieved by increasing the depth of the blade root and by increasing the almost rigid rotor head, and the blades are shortened by the same amount. The increase in the rotor head however can only be done to a slight extent because with this deviation from geometric similarity, the flapping frequency ratio is increased and the rotor becomes dynamically dissimilar in its flapping motion. The calculation of the stiffness and mass distribution of the individual blade cross sections is done on a computer. When calculating the stiffness values, the asymmetric cross sections are replaced by symmetric ones, which represent an average from the top and bottom halves. In this way, the computation accuracy of the deflection stiffness is maintained and the calculation complexity is reduced. These parameters are varied until the desired frequency ratios are achieved. /22

When selecting the cross sections, we were primarily interested in maintaining the laws of dynamic similarities. Because of

the increased blade depth mentioned above and the equalizing reduction in the wall thickness of the homogeneous part of the blade, we already have a few slight deviations from the scale factor.

	BO 105	To Scale	Model Size	Dim.
Blade Chord	0.27	0.108	0.121	m
Center of Gravity Position, abs.	0.0648	0.02592	0.02783	m
Center of Gravity Position, rel	24.00	24.00	23.00	%
Weight	5.54	0.8864	0.83	dN/m
Flapping Stiffness	695.00	17.792	23.57	dN/m^2
Deflection Stiffness	17700.00	453.12	557.00	dN/m^2
Thrust Stiffness	630000.00	100800.00	90000.00	dN/m^2

2.1.3 Distribution of the Masses and Stiffness over the Radius /23

From the values of the individual cross sections, one determines the masses and stiffnesses over the radius (see Fig. 19a, 19b). From Fig. 19b one can see that only in the case of the deflection stiffness is there a stiffness reduction in the area where the deflection hinge is usually found.

The values given in the region of the rotor head are scaled reductions of the main design. Since in the case of the model the rotor head is made of steel and not titanium, the running weights and stiffnesses with the higher specific weight and the higher elastic modulus of steel compared with titanium have been considered.

The support of the blade connection at the rotor head by two radial bearings requires consideration of the double beam when calculating the stiffness distribution. According to model laws, the spring constants of the two bearings are only linearly reduced.

2.1.4 Results of the Frequency Calculation

Using a program for calculating the flapping eigen frequencies and the deflection eigen frequencies of a bending support, it is possible to determine the required frequency ratios. The cross sections at the blade root are varied until the desired frequency ratio of the first deflection mode is achieved. In addition, frequency calculations with different blade weights were performed, which assume a 5% manufacturing tolerance. An increase in the weight by this percentage makes the first deflection eigen mode be reduced from $\omega_{1\zeta}/\Omega = 0{,}716$ to 0.6985. Therefore, it would be closer to the data of the BO 105.

When determining the flapping eigen frequencies, variation calculations over the radius with an additional mass of 0.064 kg were performed (corresponding to 1 kg in the full scale design).

For a distance of r = 0.9 m, the flapping frequency ratios agree with those of the BO 105 up to the third eigen mode. /24

2.1.5 Errors in Blade Manufacturing and Their Effects

Here we will give a qualitative discussion of several errors which can occur when manufacturing hingeless rotor blades.

When the rotor blades are scaled down, the manufacturing tolerances have to be reduced to scale. This requirement can usually not be satisfied in most cases, because already in the original version one attempts to make deviations from the nominal dimensions as small as possible.

Contour errors from the blade profile, especially at the leading edge and the trailing edge, which are not eliminated during manufacturing, have a much greater effect on the models than for the original blade, because the absolute

error remains the same. Contour errors of the blade profile produce strong vibrations at the rotor head, especially for fast forward flight. This is because compressibility effects become intensified with increasing speed.

Fig. 20 shows the effects of manufacturing inaccuracies on the center of gravity, the blade sweep at the connection bolts, the blade twist, and the trailing edge shape and how they affect tracking, weights and control forces of the rotor. Since there are various operational states for helicopters (running on the ground, hovering flight, cruise, flying curves) we investigated the effects of the inaccuracies mentioned above.

2.2 Design and Construction of the Rotor Head

In the full scale design of the rotor head, the parts which define the strength and the stiffness and the rotor star as well as the inner shells are made of titanium in order to save weight. /25

Single fabrication of these parts of the rotor model made of titanium would result in major expenses and major time requirements which are not jusitified.

Since these parts only experience unimportant elastic deformations and they only produce small dynamic mass forces, they were made of steel in the model. The higher specific weight and the larger elastic modulus of steel compared with titanium does not lead to impermissible deviations from the dynamic similarity of the model rotor in these stiff parts, if the distance is maintained with geometric similarity between the blade main bolts and the axis of rotation.

In the case of the hingeless rotor, there is a rotating hinge (Fig. 21) in the rotor head, in order to incline the blade. Since there are no other hinges, they experience a greater load than for a rotor with a hinge. The inner shells connected with the blades, therefore, have to be supported in the radial and axial directions of the blade. In the case of the model therefore, needle bearings with small dimensions and relatively large carrying capacity as well as low torsion tension members for absorbing the axial forces can be used in the model just like in the full scale version. In this way, similar geometric conditions are achieved as are found in the full scale version of the rotor head.

Then it is important, when arranging the radial bearings, to absorb the flapping and deflection moments with as little play as possible and to have a large axial separation of the bearing centers from one another. Since the model size of the needle bearings, however, is relatively large compared with their carrying capacity, special design features are required considering the given size of the model rotor head in order to approximately satisfy the geometric conditions of the full scale version.

In order to make the tension members have as little torsion resistance as possible, it is required to make them as long as possible. Since the model size of the tension members however requires a substantial axial length for their connections compared with their carrying capacity, for a given size of the model rotor there is relatively little free length available for the torsion members and therefore special design requirements are required for this detail in order to approximately satisfy the geometric relationships of the full scale version. /26

The rotor head is screwed into the rotor shaft through a flange. Cylindrical bushings provide radial centering and transmission of the torque. The 2-blade reaction rotor can also be used with this rotor shaft using the same flange connection.

2.3 Blade Manufacturing and Final Assembly

First of all, a two-part negative crest mold is made, which insures that the blade profile is maintained and that there is geometric similarity of all of the blades (Fig. 22).

The two mold halves are designed with a tissue skin 0.4 mm thick over the entire blade length and this is wetted with the prescribed weight of resin. After this, several layers of tissue are applied at the blade throat and are impregnated with the prescribed amount of resin. Finally, five rowings of the homogeneous part are laid into each half around the grommet and this is set into the profile mold using a templet. Then the short rowings are laid in around the blade neck. Then the lead strand and the trim chamber are installed at the end of the blade using a holder. The rowings remain in the preheated mold, heated to 45°C, for about 4 hours. There, they gell and become solid somewhat. Then the two halves of the foam core are impregnated with a small amount of resin and inserted into the molds. These two halves of the mold are closed and tensioned. Finally the mold is held in a hardening oven for about 8 hours at a temperature of 100°C. The raw blades after removal from the mold are cleaned, and the nose shell and the end shell are laminated on in the blade throat area. The nose shell is checked with a templet and is ground down to the nominal dimension.

/27

The blade is then embedded into a 2-part connection fitting with its grommet (Fig. 23), and a special device holds the position of the blade with respect to the fitting during the hardening process. Finally a cover made of GfK tissue is laminated on at the end of the blade.

The finished rotor blades are then assembled into a set of four each. One attempts to get the equal static mass moment around the rotor rotation axis. Often, extensive tests have to be performed for this, which are performed on a balancing device as shown in Fig. 24.

In order to test the dynamic similarity with respect to the BO 105, the blades were excited in the flapping, deflection and torsion directions at $\Omega_{RO} = 0$ and their eigen frequencies were measured with DMS (strain gauges). It is found that the accuracy of the first eigen frequencies are in the area of ±3% and therefore one can assume that there is good dynamic similarity between the model and the original.

We will later on report about extensive measurements on the higher eigen frequencies and eigen modes.

Fig. 25 shows the rotor before delivery to the DFVLR.

2.4 2-Blade Reaction Rotor

In spite of its thick blade profile a reaction rotor has good possibilities of investigating the efficiency of blade modifications. Therefore, one central point of the wind tunnel investigations was the following. /28

- Investigations when mixing blade tip drive and shaft drive
- Modification at the air exit point at the blade tip

- Variations of the blade tip shape
- Flap control for higher harmonic aerodynamic force components.

Because of the simple design of the blades made of a strand-cast-pressed hollow profile it is possible to perform pressure distribution measurements over the blade contour without any measurement difficulties. In contrast to the 4-blade Gfk (glass fiber reinforced plastic) rotor, pressure sensors and cables can be laid in without any problems. The sensor weight divided by the blade weight is a very favorable ratio, so that the blade eigen frequencies are hardly changed at all. By using an easily removable blade tip section, one can then optimize the profile shape without much complexity.

2.4.1 Rotor Head (Fig. 26)

The rotor head is a semi-rigid 2-blade rotor with a central flapping hinge. Two forks which are connected to spring packages in the rotor support the rotor blades and absorb the centrifugal forces as well as the flapping and deflection moments. The gas is let out to the side from the rotor head and runs to the center of the fork through a tube, so that the gas flows through an intermediate part into the rotor blade. The gas supply tube is designed so that the rotor control and the resulting blade motion does not impart any bending moments on the tube. The rotor hub is made in two parts due to assembly considerations. The flapping hinge is supported on the gas distribution tube. This is flanged onto the rotor mass and is then used to support the rotor. The blade displacement is provided by two oil lubricated roller bearings. The flapping hinge and the sealing bearings are filled with grease.

In order to reduce the Coriolis forces, the rotor has an /29
"underslung" configuration. In other words, the flapping

axis is above the intersection point of the blade torsion axis. Therefore the centrifugal forces above the flapping axis produce a different direction of rotation than they do below it. This, then, leads to a reduction in the Coriolis forces during the flapping motion.

2.4.2 Rotor Blades (Fig. 27)

The rotor blades consist of a strand-pressed light metal hollow profile. The blade connection is glued on as a lamella construction to this profile. The trailing edge is designed as a light metal sandwich web construction and is also glued on. There is a round nozzle screwed into the blade tip, which provides for rotor drive. The rotor blades are twisted (5°/m) and have a cone angle of 0°54' with respect to the horizontal. Therefore, only small bending moments occur in the flapping direction in the blade fork during hovering flight and the load factors are n = 1.

2.4.3 Hybrid Drive

One special feature of the rotor is the possibility of investigating combinations of blade tip drive and shaft drive. If the rotor is to be driven pneumatically only, then a pressurized air generator must produce the required amount of air of 1 kg/s at a pressure of 2.65 bar. The temperature of the air will then rise to about 424°K (about 150°).

Fig. 28 shows the design of a hybrid drive for the rotor test stand.

The hydromotor and the air supply are attached to the rotor shaft along the lower plate. There is an electrical brake on the plate, which can stop the rotor if only the pneumatic drive is used. Above this there are five pulley disks, which

are connected to the hydromotor with V belts. After this, there is a cog belt disk with a cog belt, which drives a tachogenerator, and therefore provides information about the rotation rate and the rotor position. /30

Except for a changed hollow rotor shaft, all other parts of the rotor carrier and the control system can be retained.

During the test program of the 2-blade rotor, in 1983 we will carry out a test stand test program, which will provide information about the performance of the rotor with different drive conditions. Then operating points with different fractions of pneumatic drive and shaft drive will be investigated. Finally, we would like to point out that the rotor has a higher resistance and therefore a higher power requirement than does the 4-blade rotor because of the fixed blade profile and the flow losses. However, in the case of the helicopter this could be different, because blade tip drive does not require any torque equalization by the tail rotor. During hovering flight, the power requirement of the tail rotor is about 10% of the total power. The power requirement however decreases with increasing degree of advance because of the influence of the wing.

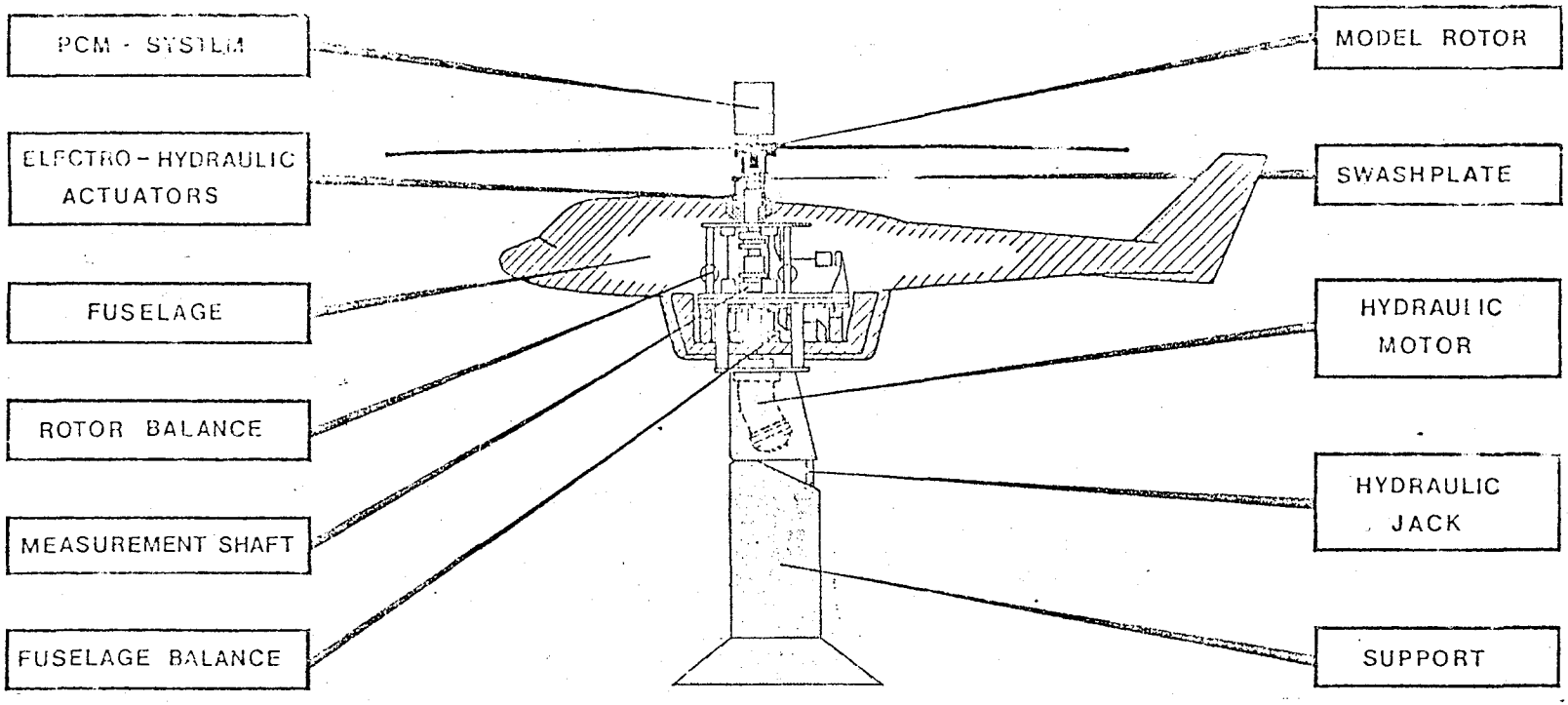

Fig. 1: HELICOPTER TEST STAND

Drive System

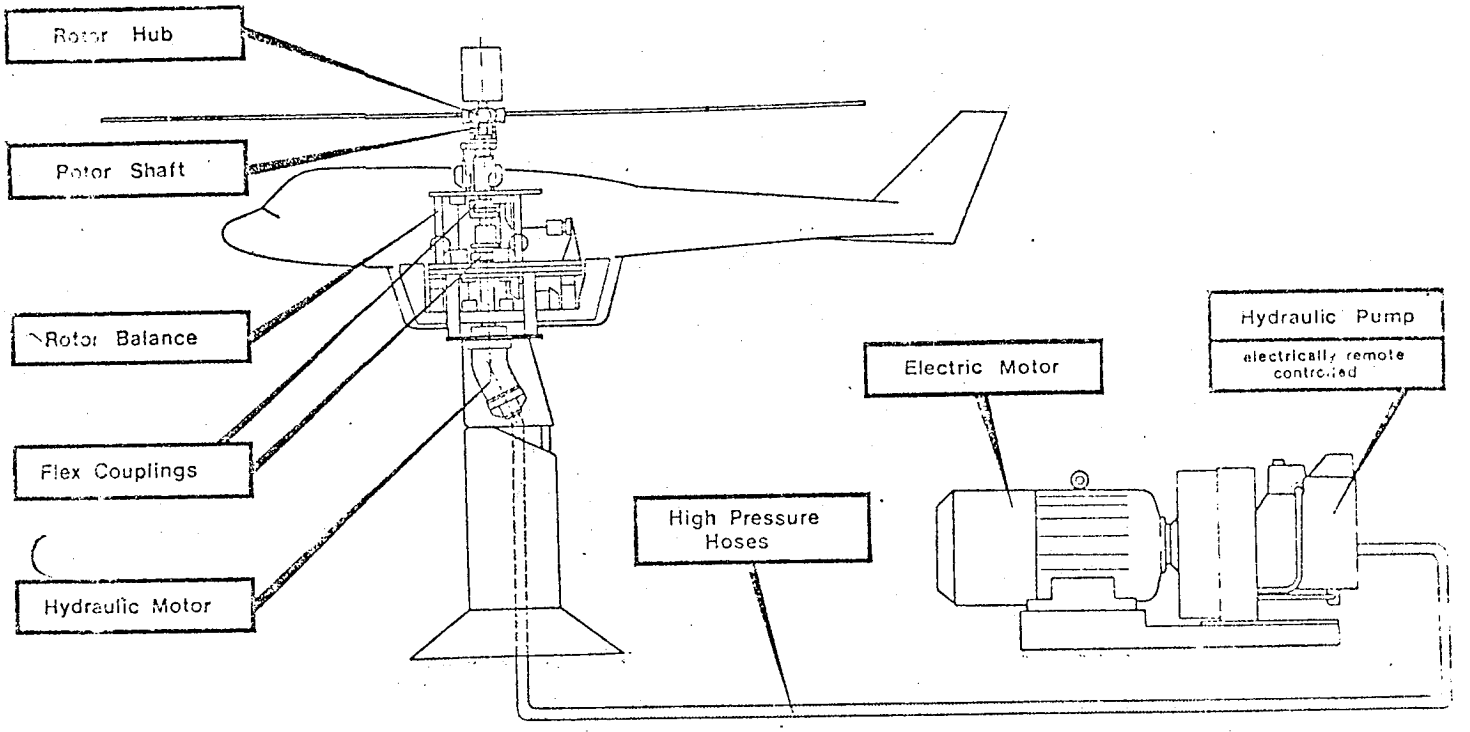

Fig. 2: Drive System of the Rotor Test Stand

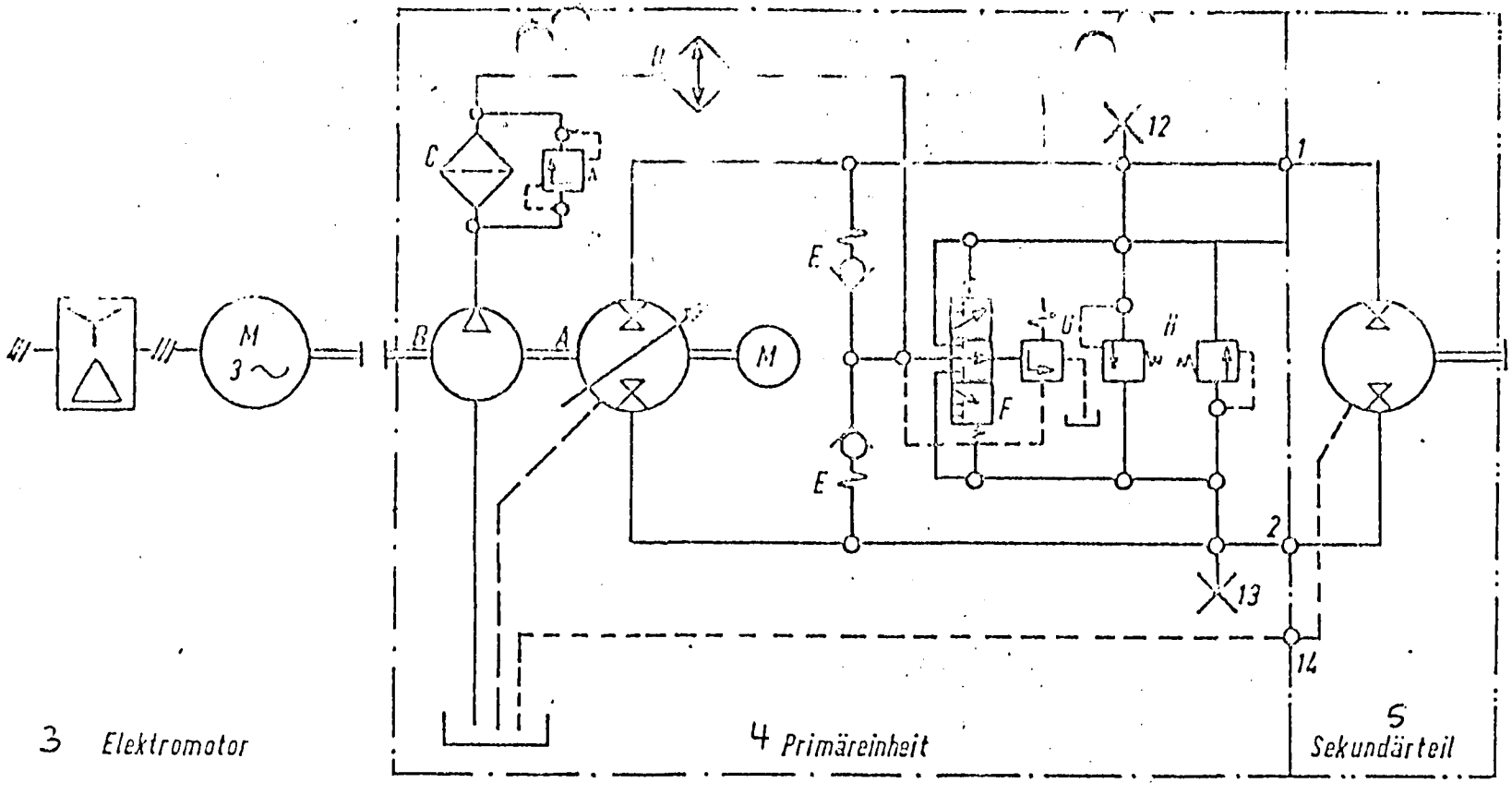

A. H.G. Unit with electrical adjustment (rpm)
B. Supply Pump
C. Filter
D. Cooler
E. Supply valve
F. Rinsing valve
G. Supply pressure valve
H. Double acting over pressure valve

10. Connections for secondary part
1. High or
2. Low pressure connection
12. High and low pressure -
13. Manometer connection
14. Reverse flow connection for oil leaking from the oil motor
3 - Electrical motor
4 - Primary unit
5 - Secondary unit

Fig. 3: Circuit diagram of the hydraulic drive unit

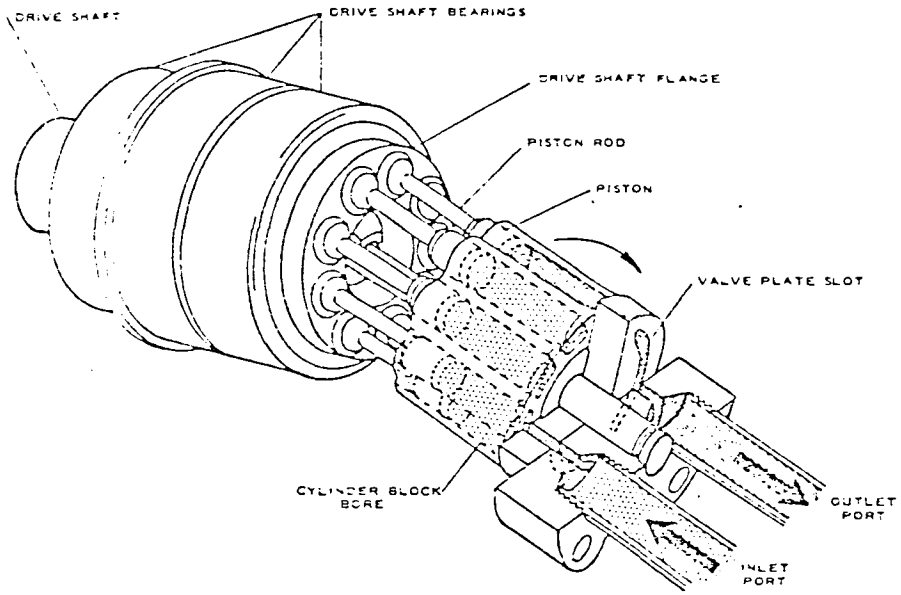

Fig. 4: Principle of a hydraulic motor

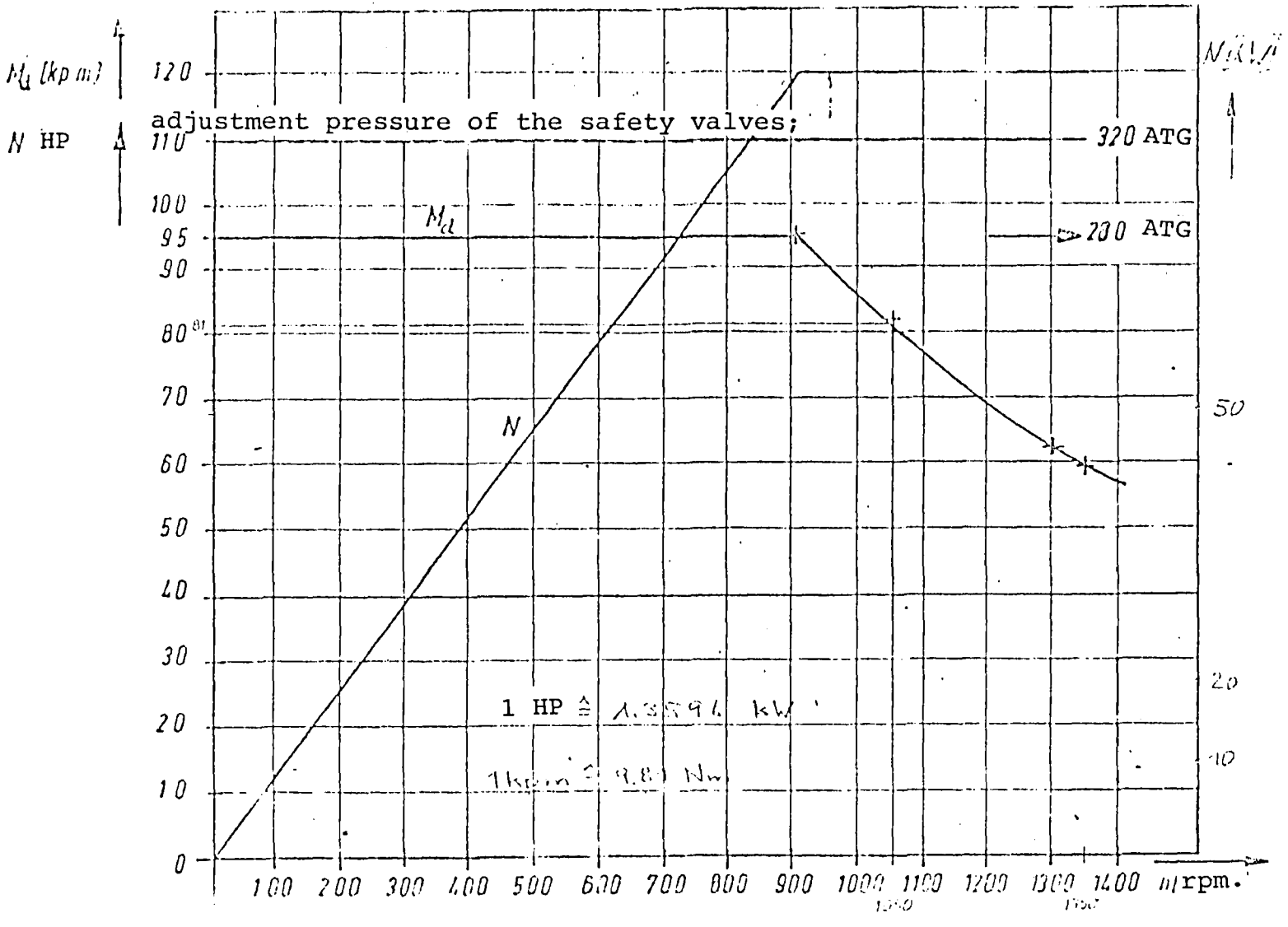

Fig. 5: Power distribution and torque variation with rpm

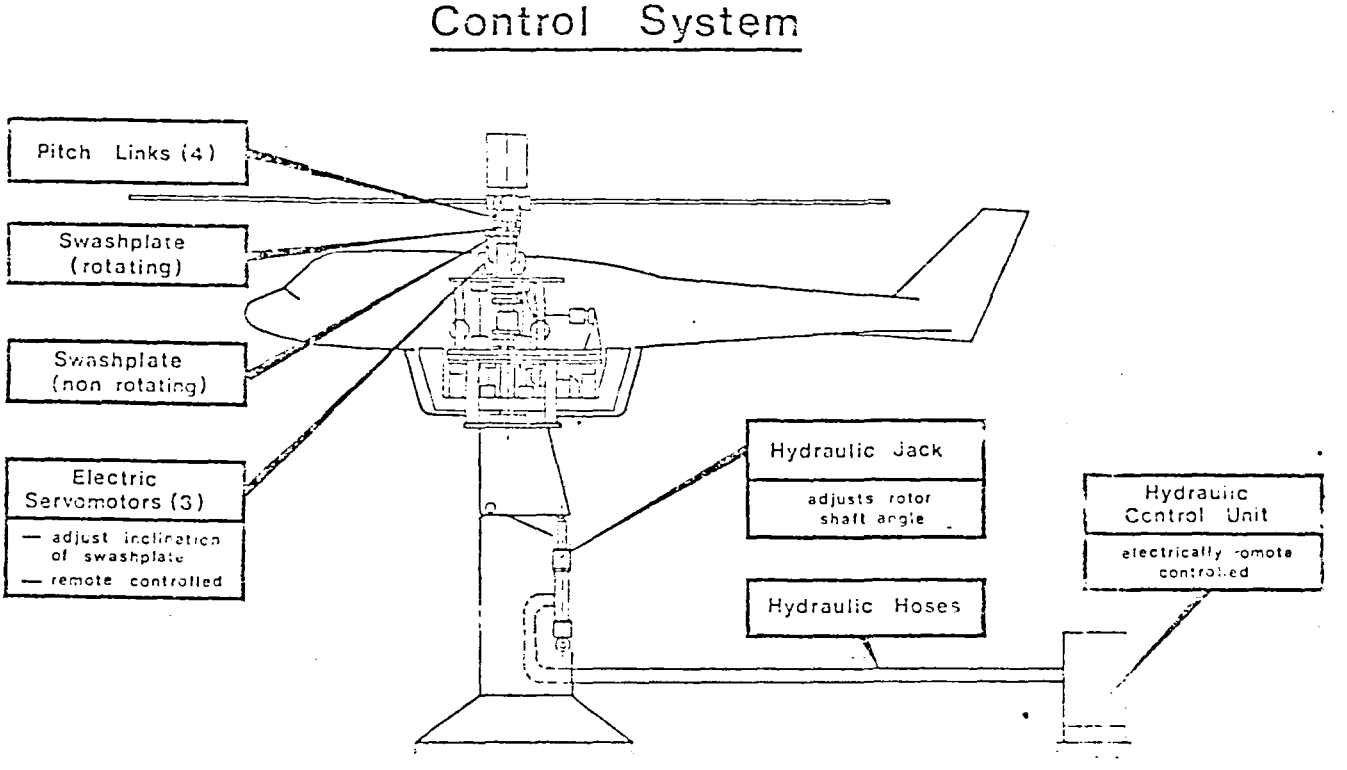

Fig. 6: Control system of the rotor test stand

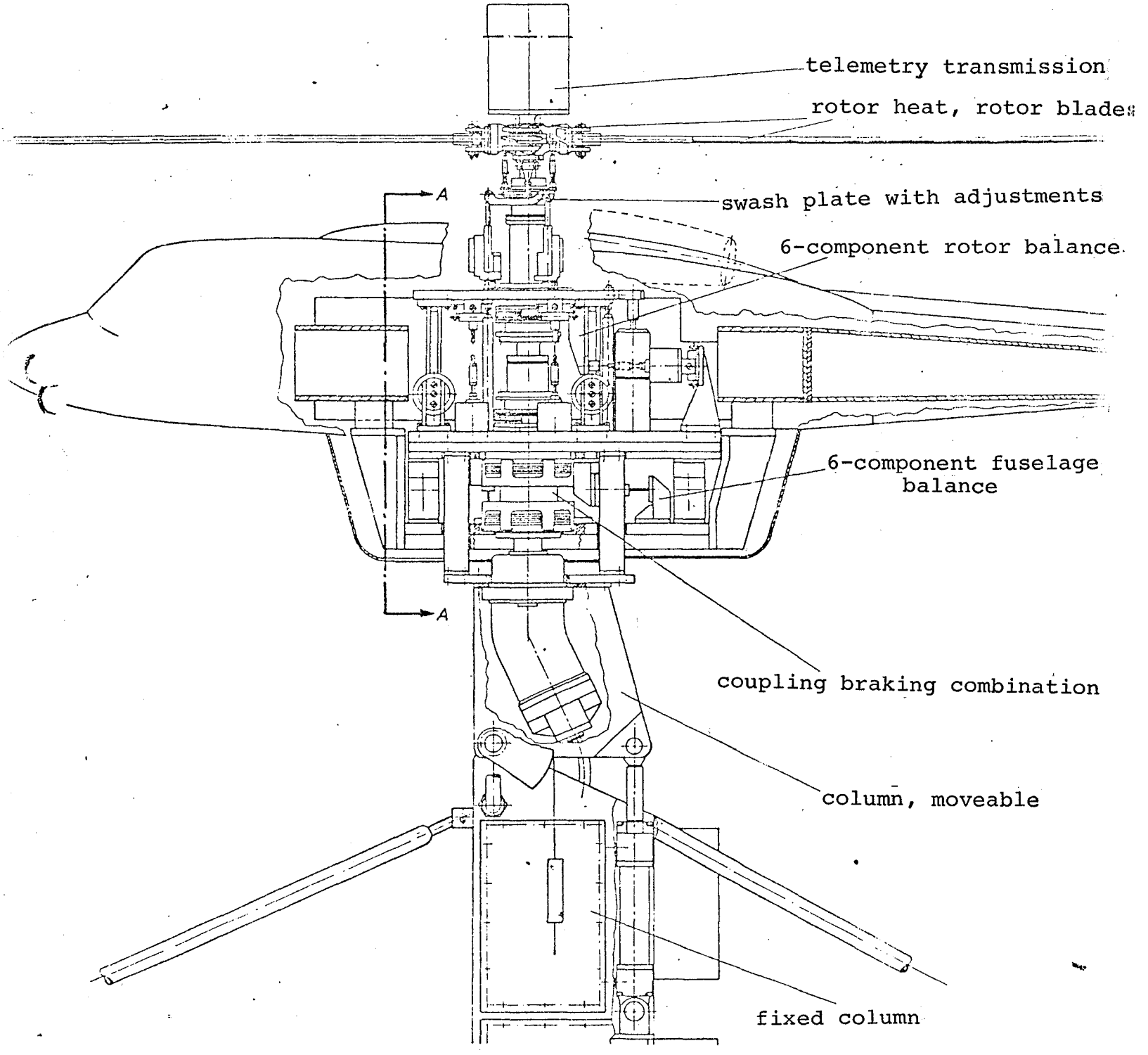

Fig. 7: Rotor balance and fuselage balance on the rotor test stand

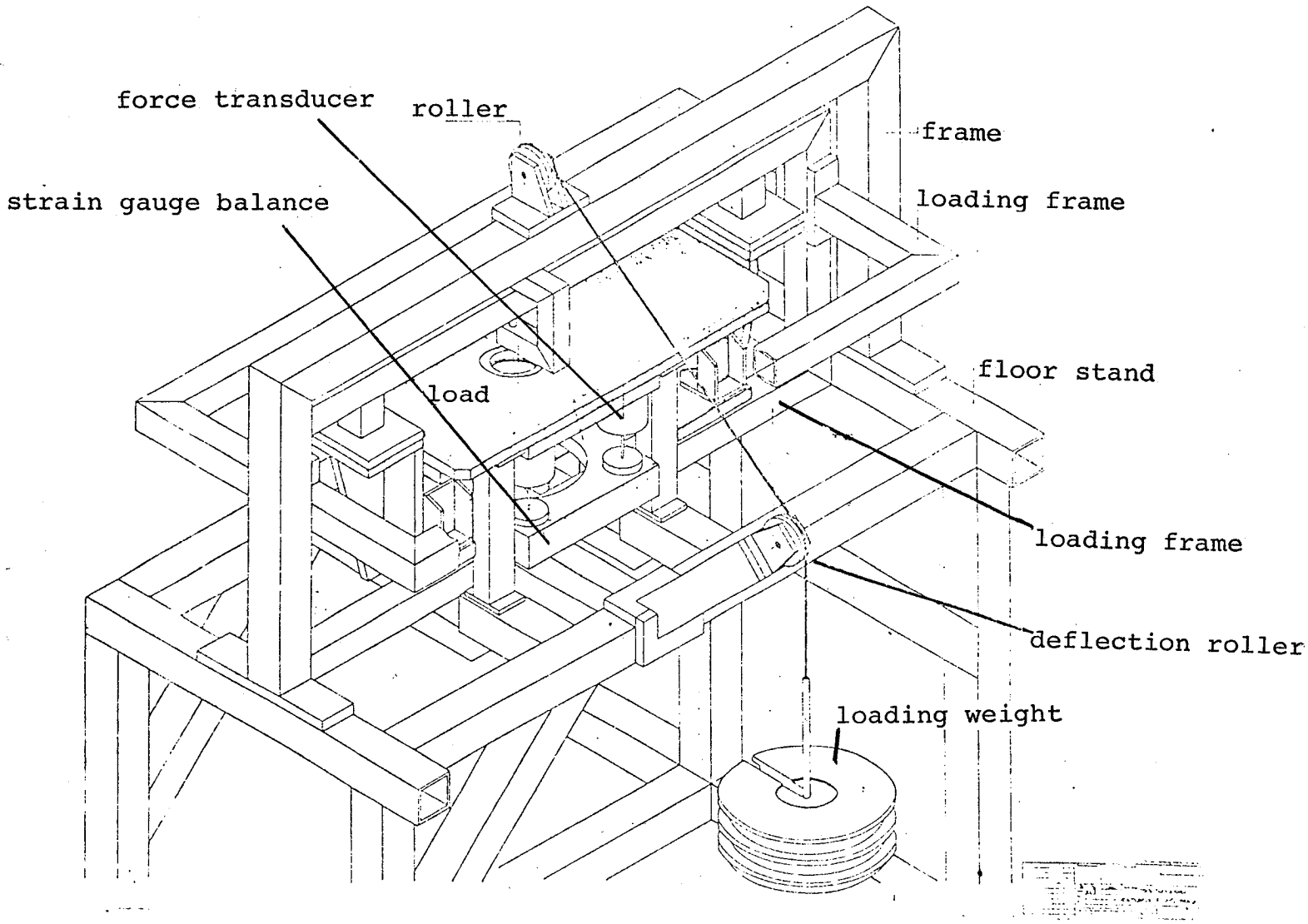

Fig. 8: Calibration unit for a strain gauge balance
(fuselage balance)

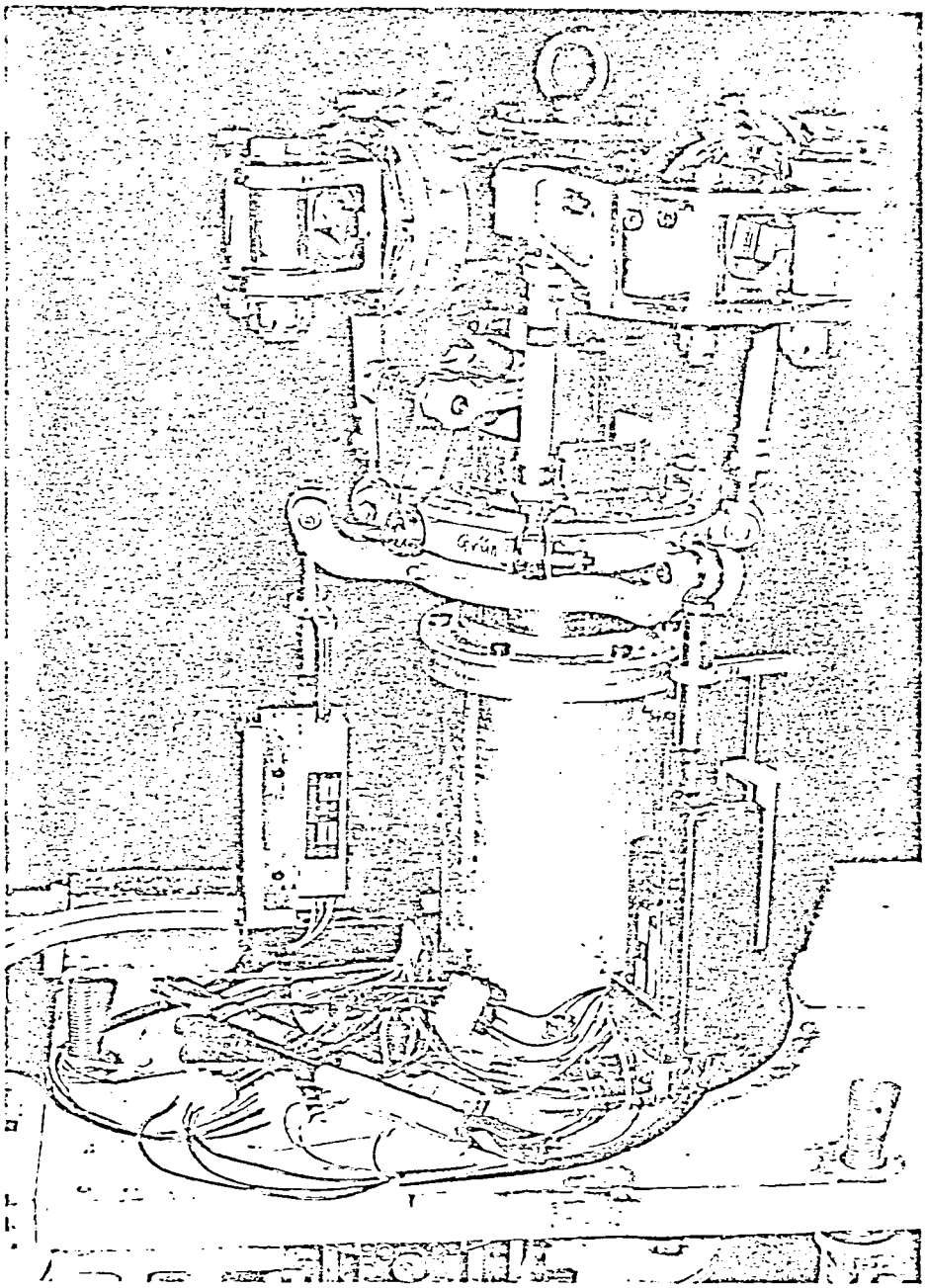

Fig. 9: Blade control

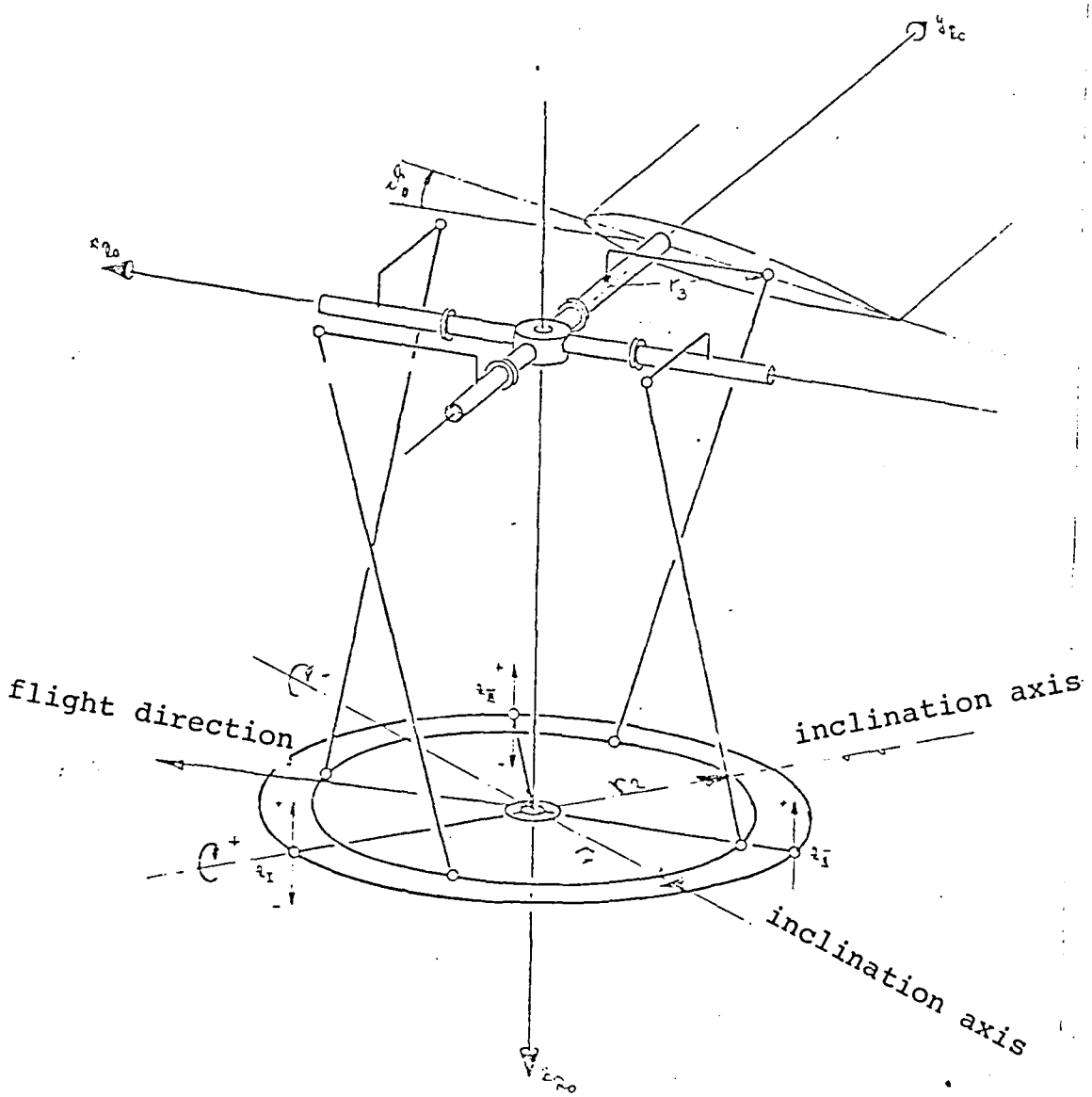

Fig. 10: Relationship between swash disk position and blade angle variation

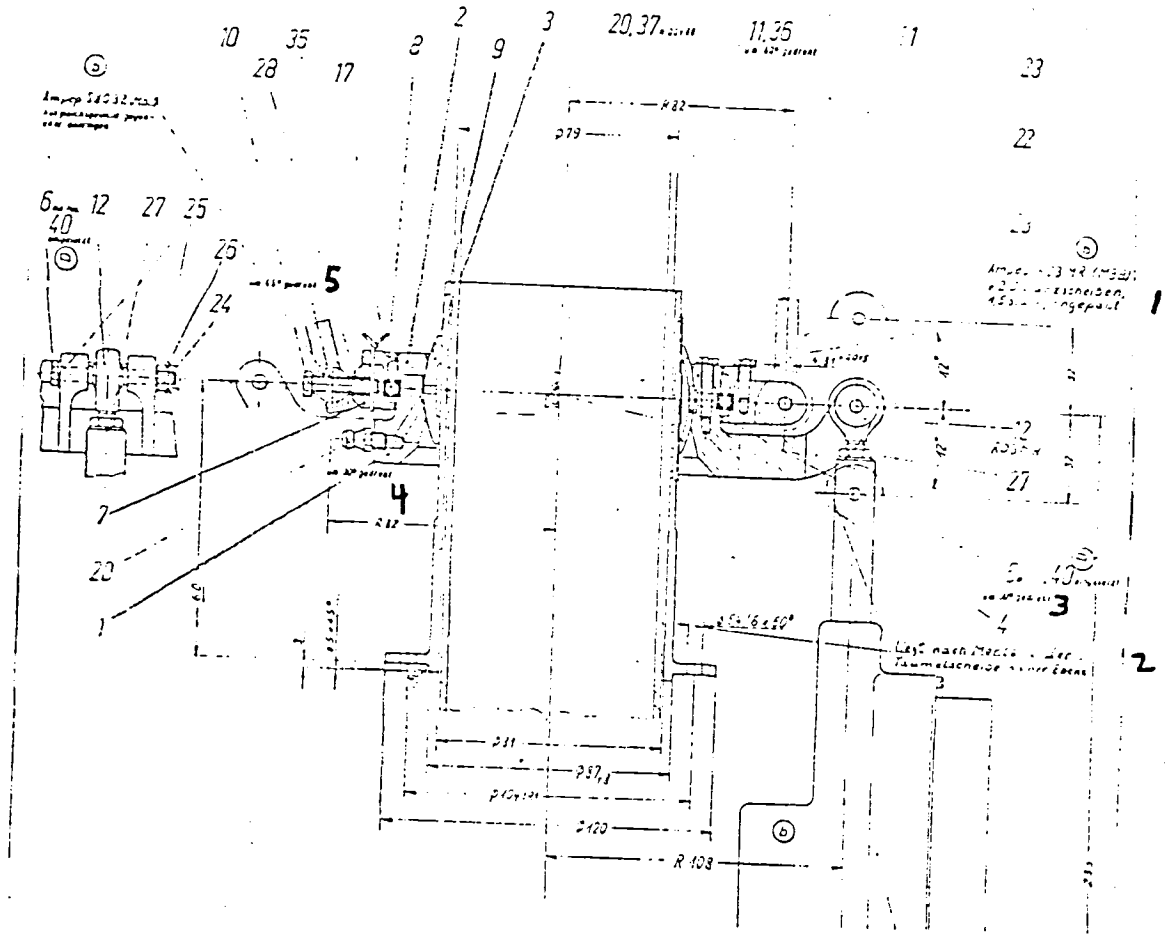

Fig. 11: Swash plate with cover

1 - 2 separation discs, 1.5 thick, adjusted; 2 - after installation of the swash plate, this is in a plane; 3 - rotated by 30 degrees; 4 - rotated; 5 - rotated

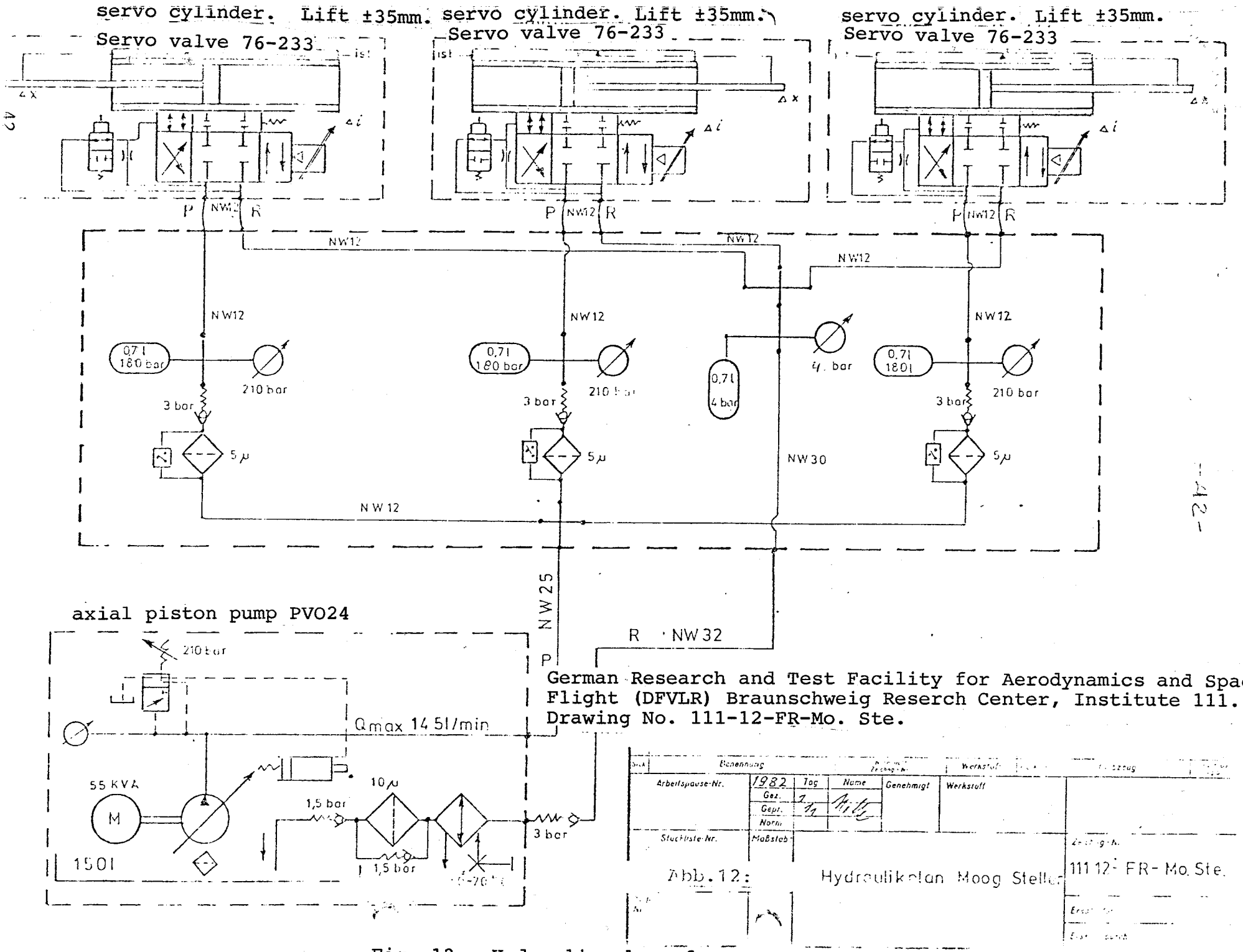

German Research and Test Facility for Aerodynamics and Space Flight (DFVLR) Braunschweig Reserch Center, Institute 111.
Drawing No. 111-12-FR-Mo. Ste.

Fig. 12: Hydraulic plan of moog actuator

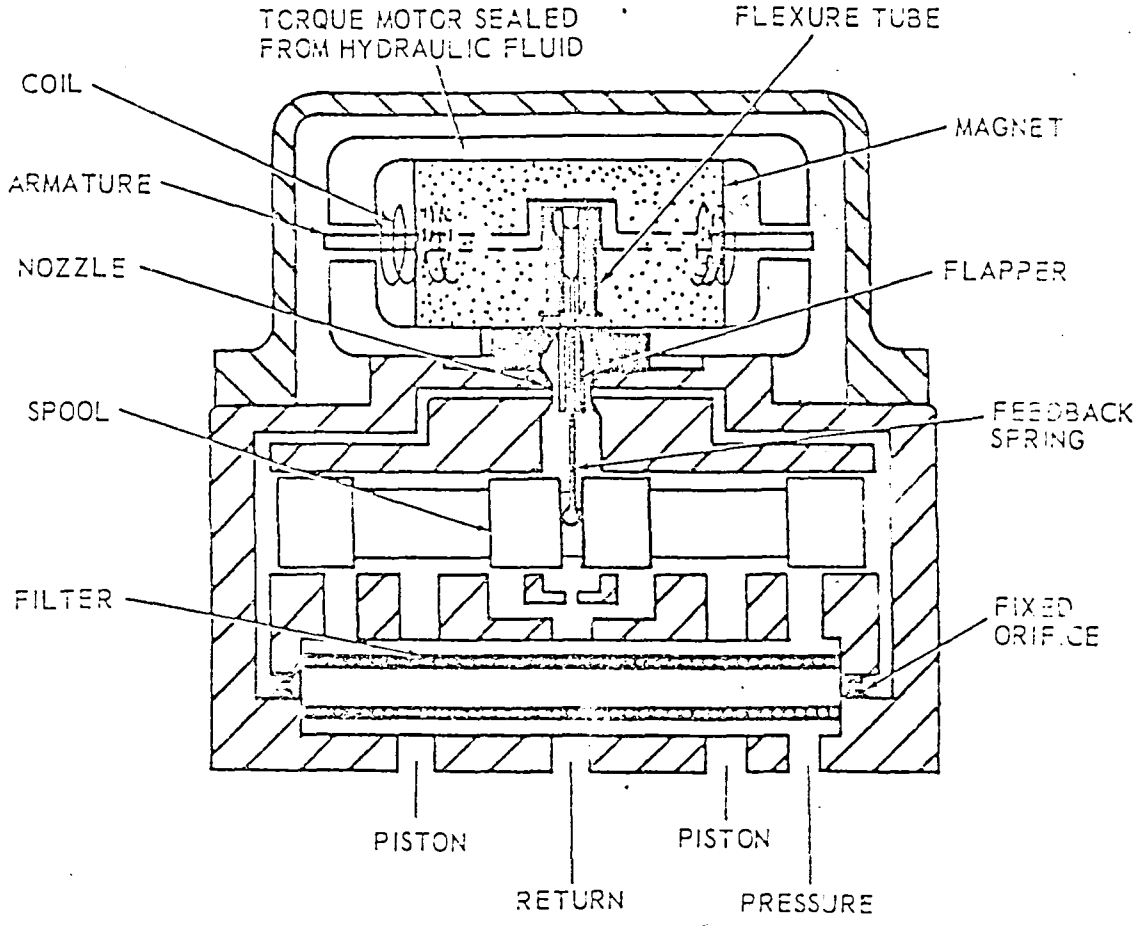

Fig. 13: Servo valve with servo motor

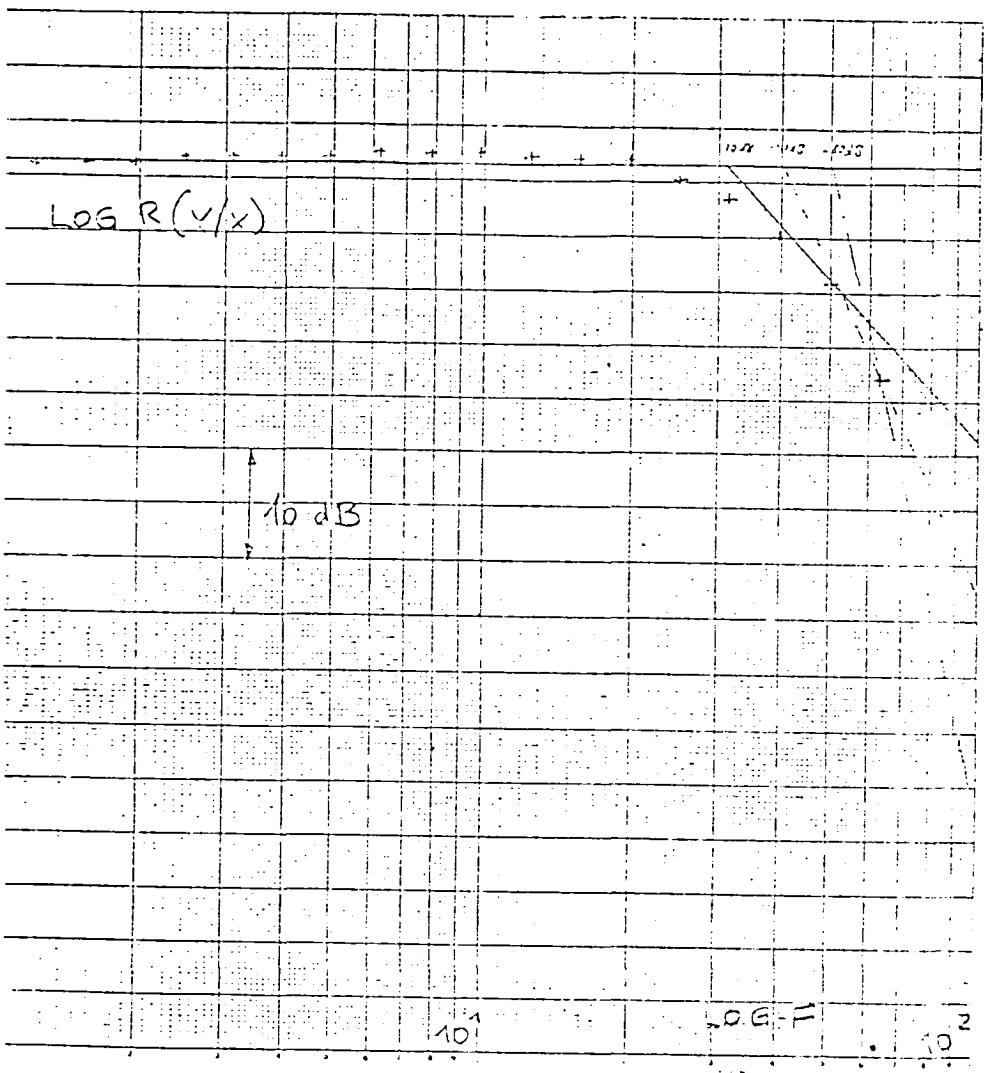

Fig. 14a: Amplitude variation of a hydraulic actuator

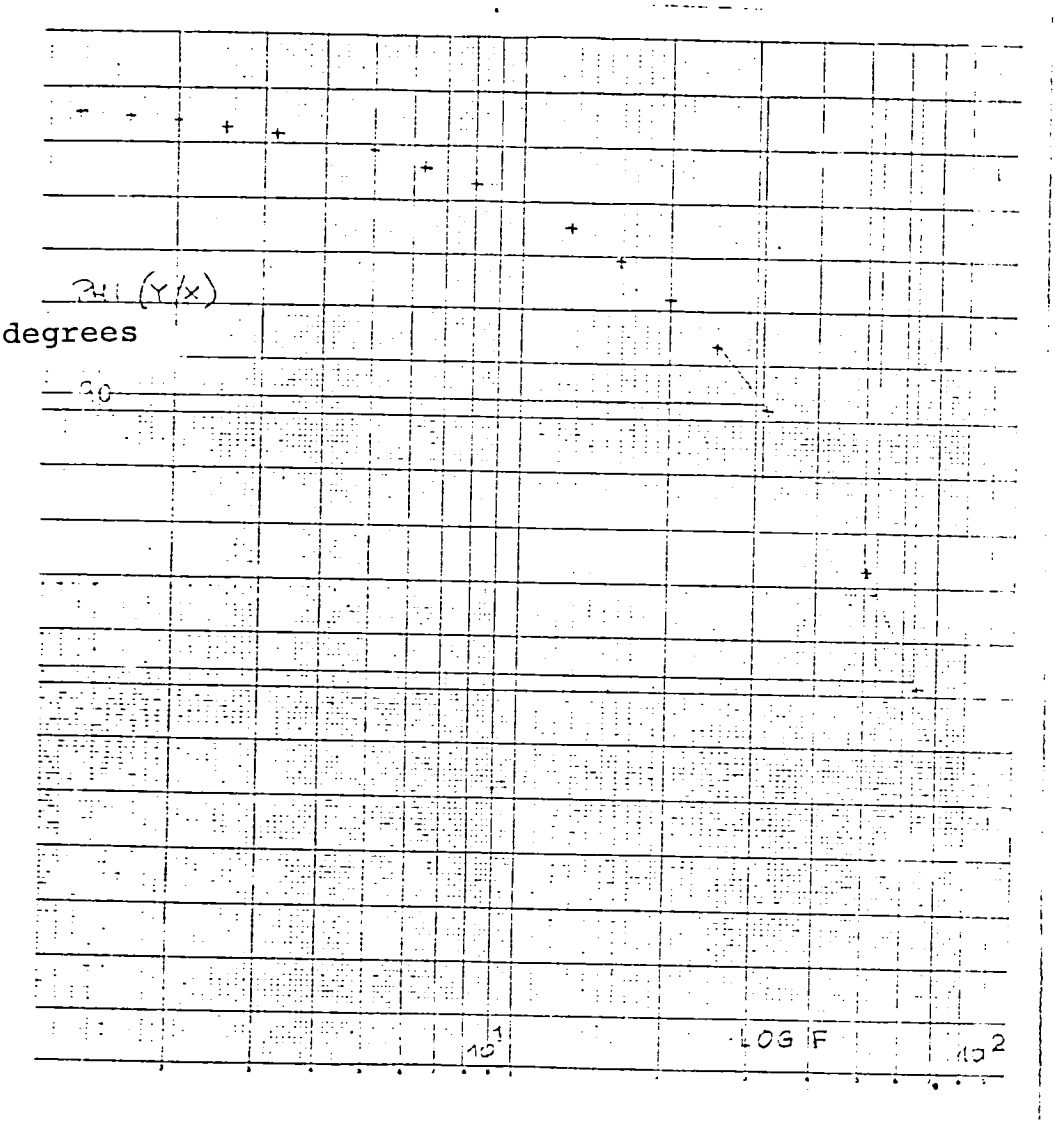

Fig. 14b: Phase variation of a hydraulic actuator

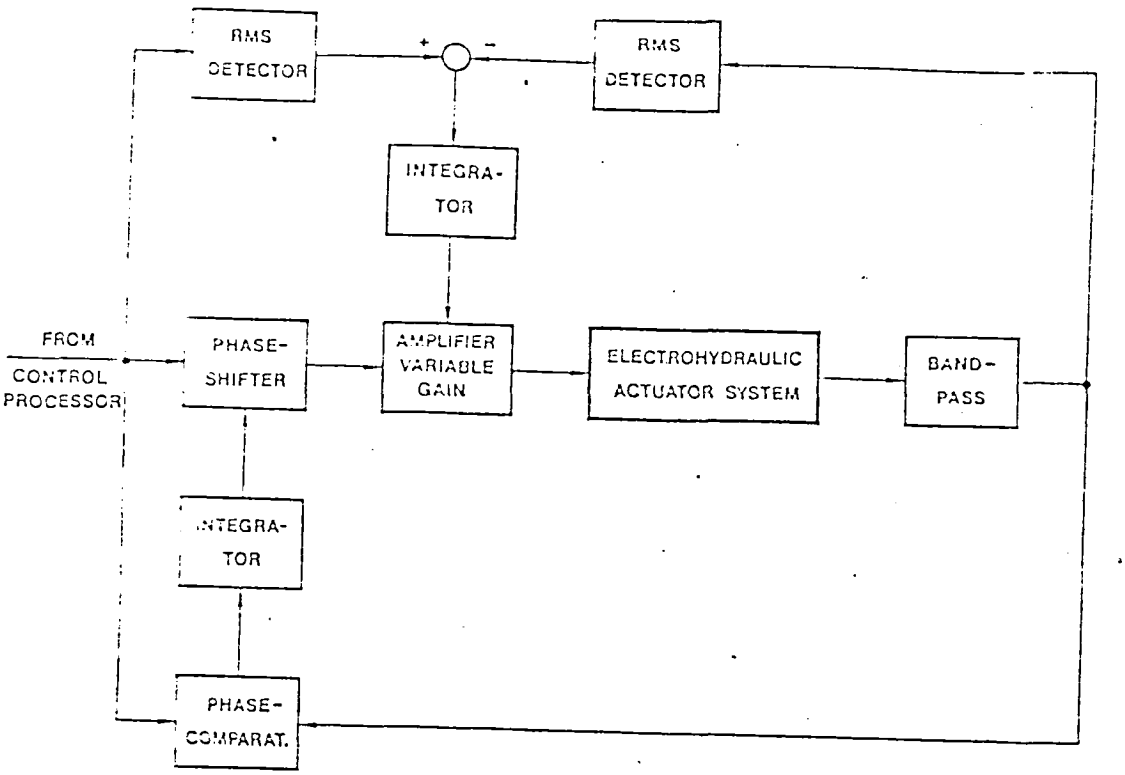

Closed Loop Control, Block Diagram

Fig. 15: Control of a hydraulic actuator system

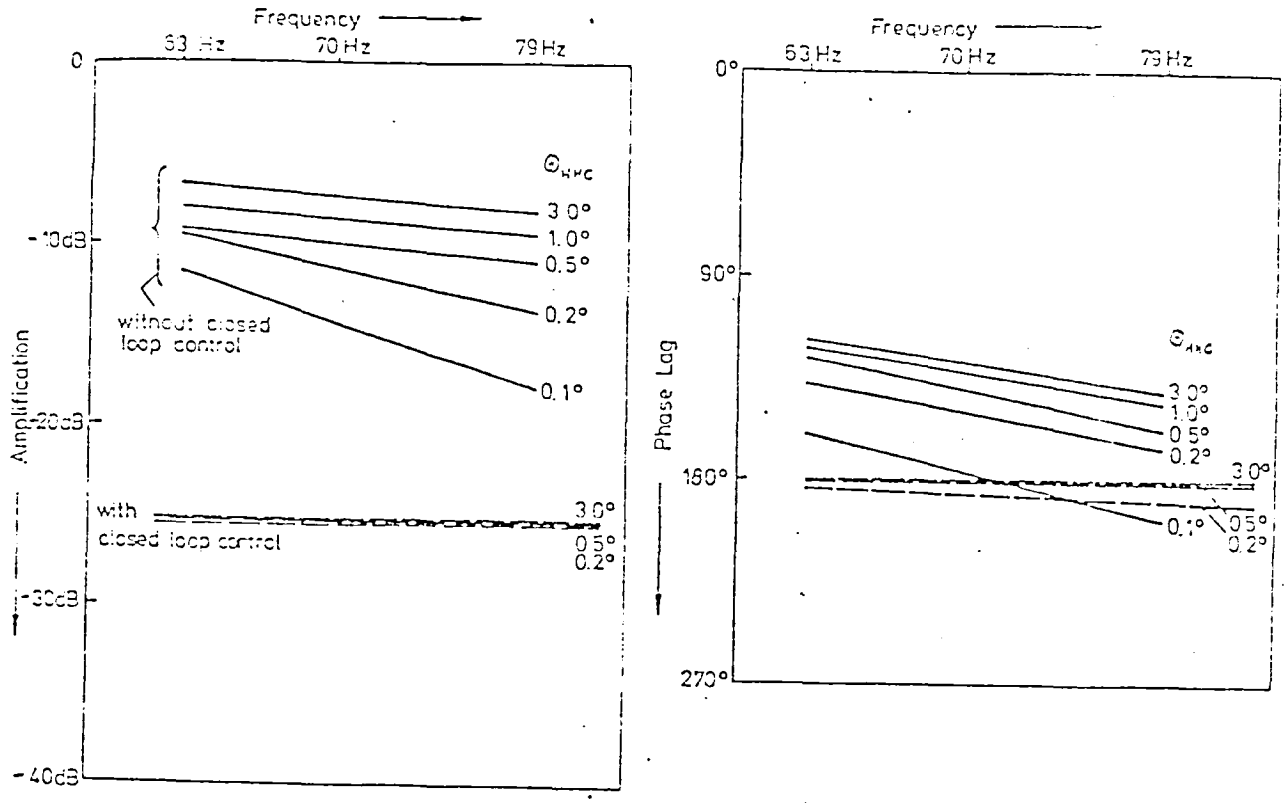

Frequency Response of an Actuator System, with and without Closed Loop Control

Fig. 16: Frequency variation of a hydraulic actuator system with and without control

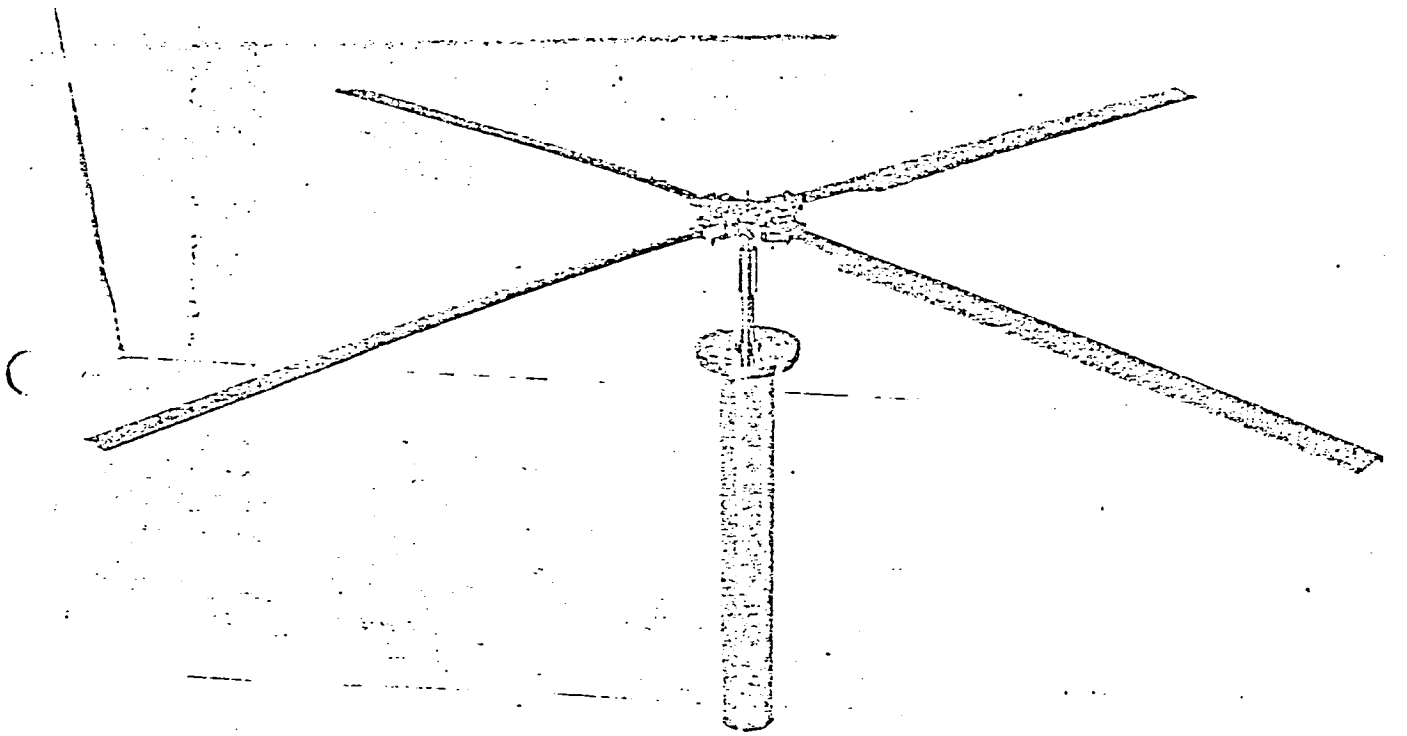

Fig. 17: Research rotor I, 4-blade rotor, hingeless

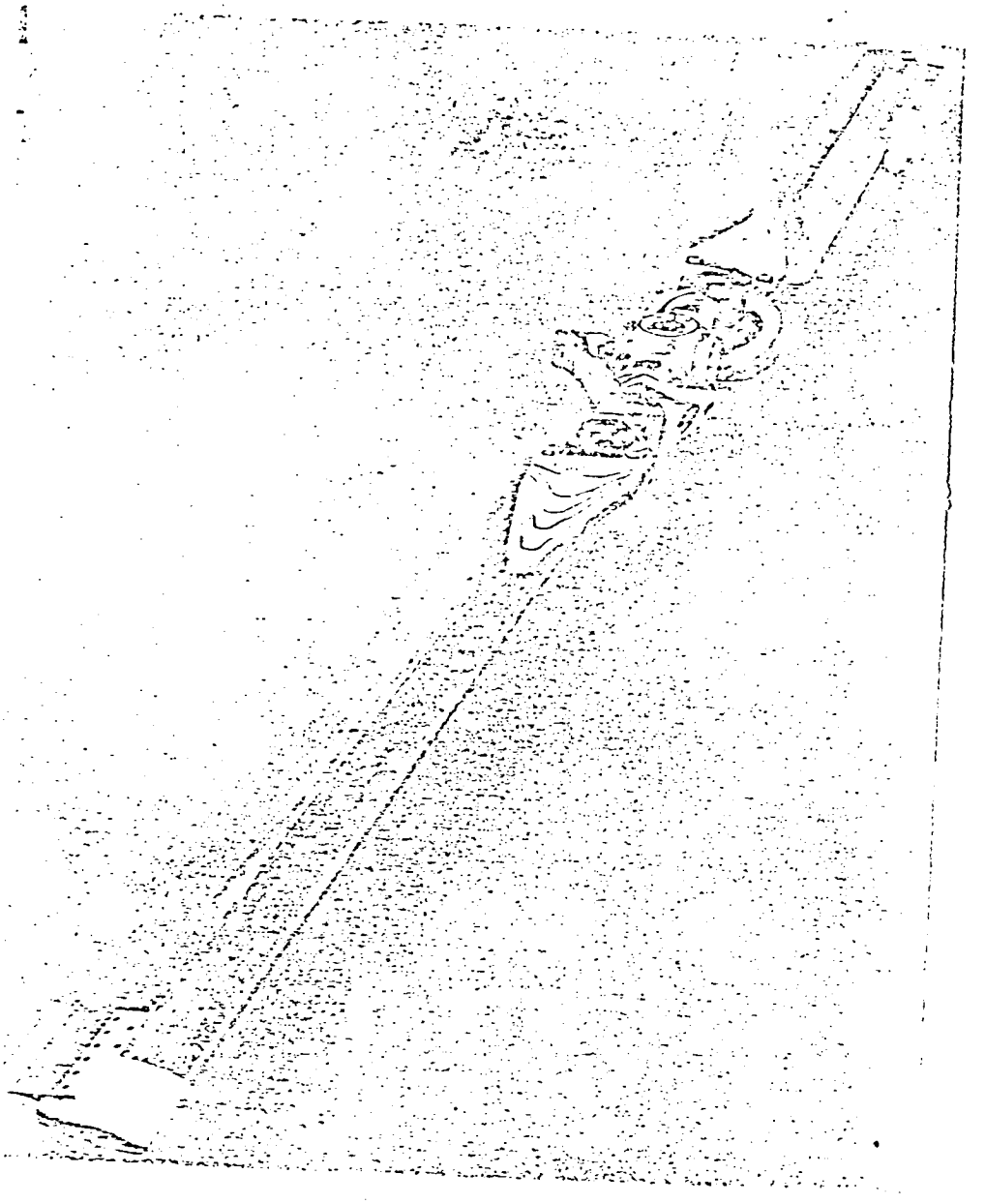

Fig. 18: Research rotor II, 2-blade rotor with central flapping hinge

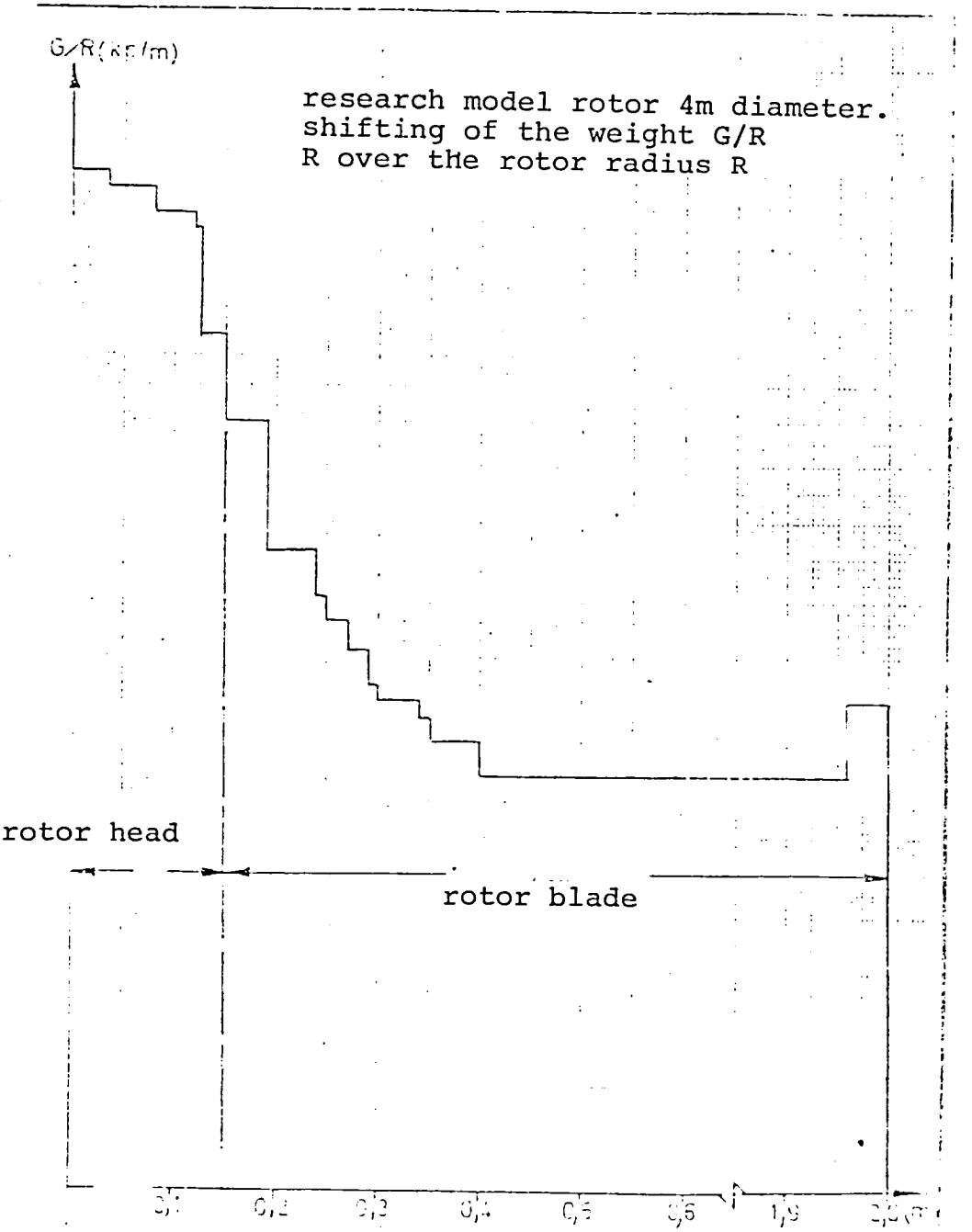

Fig. 19a: Weight distribution over the rotor radius

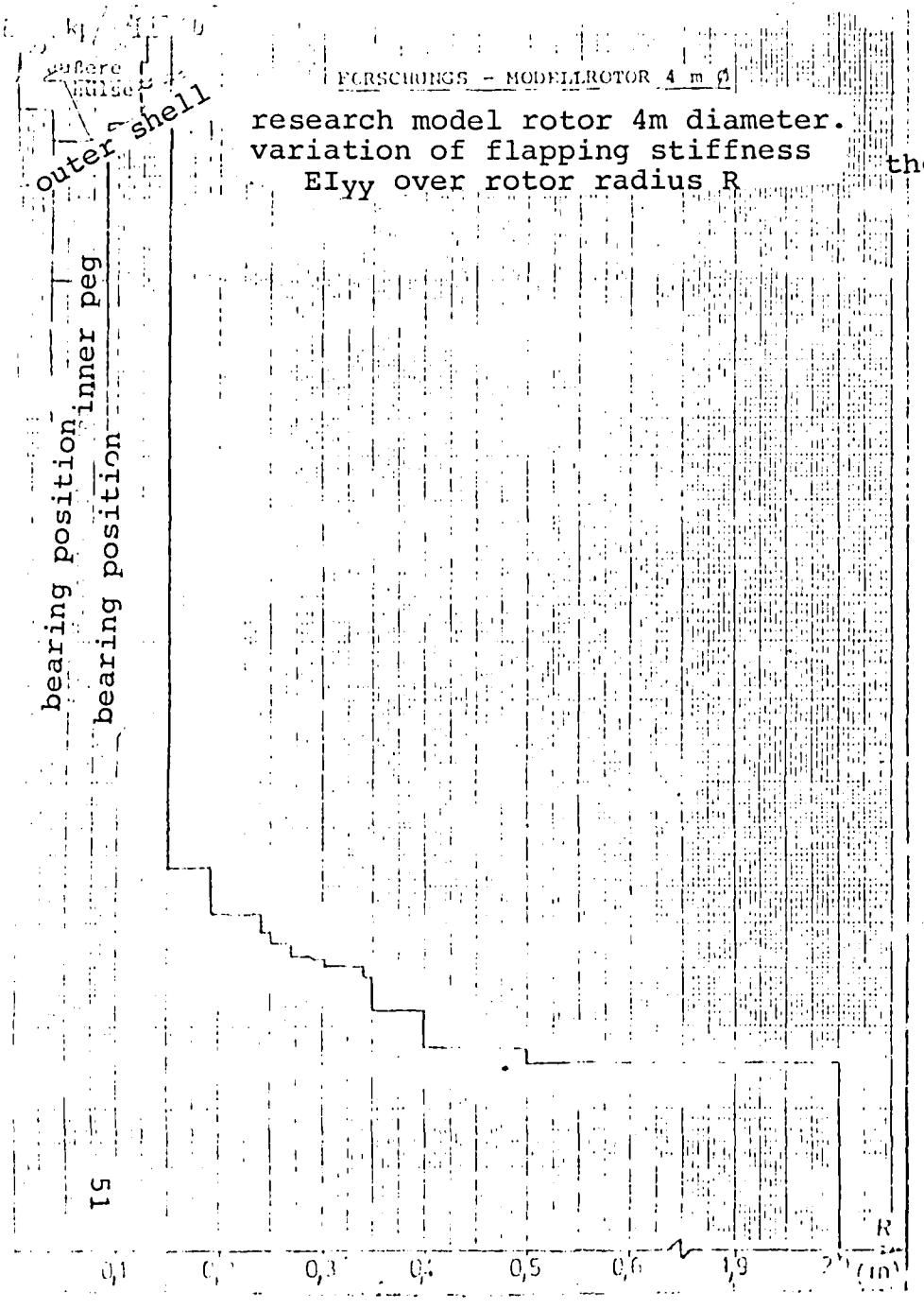

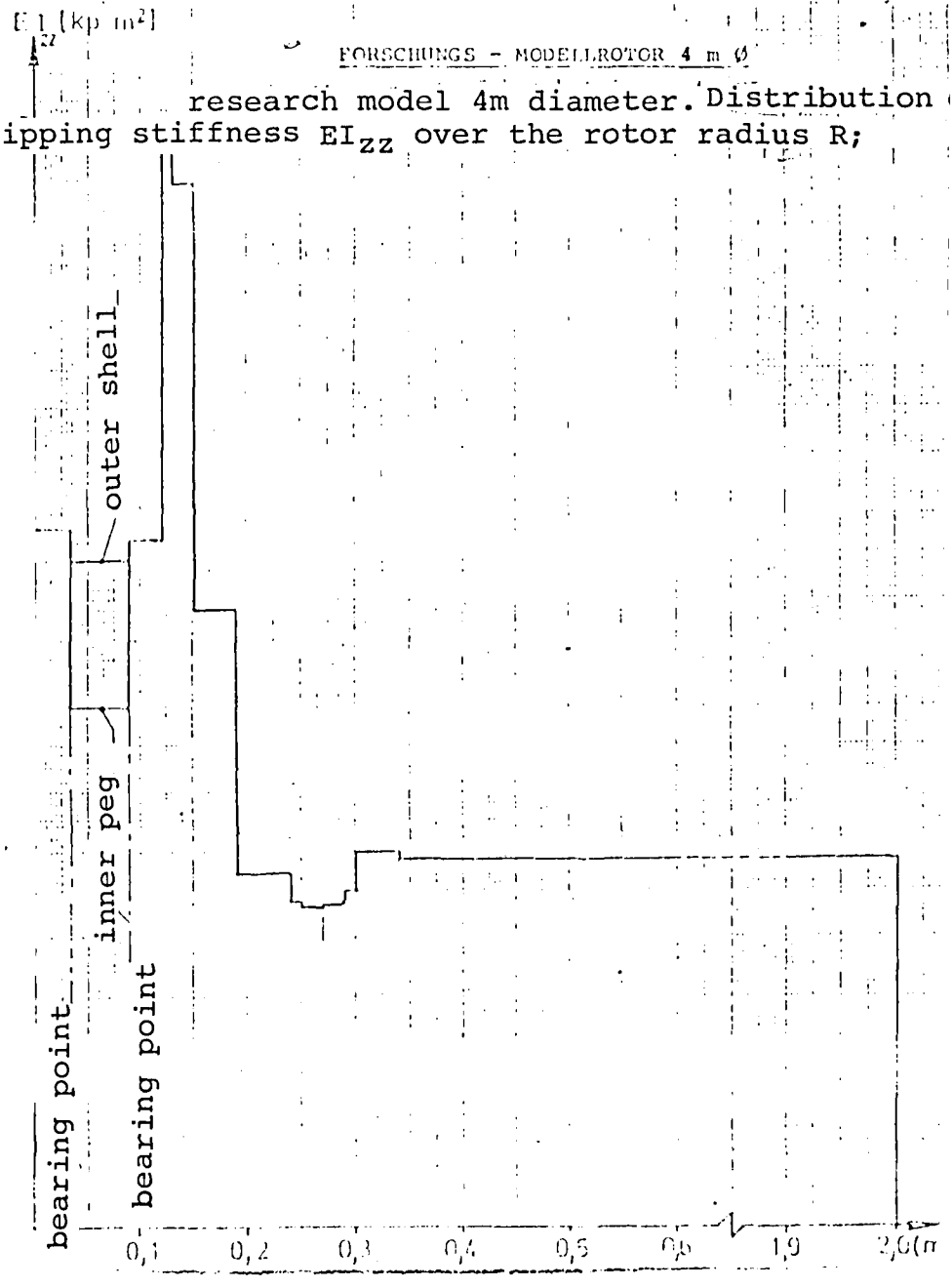

Fig. 19b: Stiffness distribution over the rotor radius

I. C.G. position in the blade stiffness direction

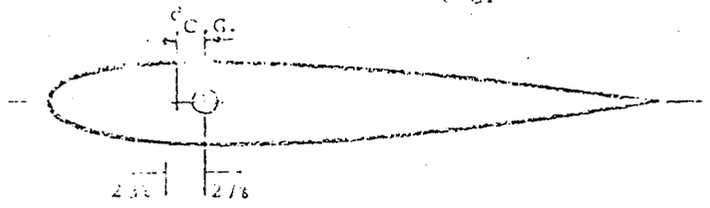

track

low position of blade center of gravity

● = great influence ◐ = low influence ○ = no influence		mass imbalance	
control force	○ ◐ ● ●	◐ ○	○ ground variation ◐ hovering ● flight cruise flight ◐ climbing curves
blade sweep edge shape	● ○ ◐ ●	◐ ○	● ◐ ○ ◐
twist	● ◐ ● ◐	◐ ○	○ ◐ ● ◐
profile trailing	● ◐ ● ◐	◐ ○	● ◐ ● ◐

cumulative arrangement of parameter influences.

ade sweep at the connection bolt

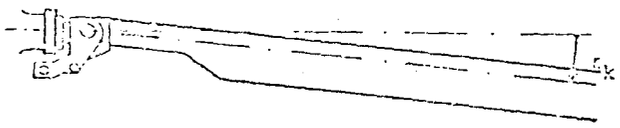

I.
ade twist

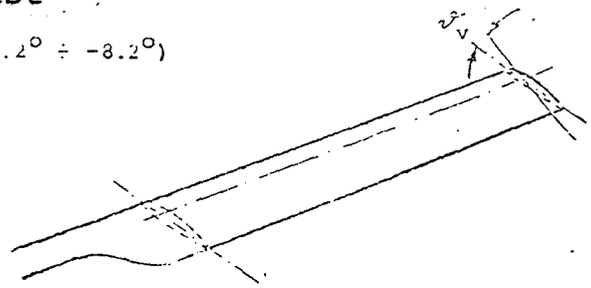

iling edge shape

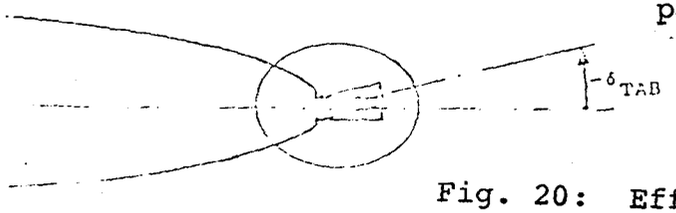

Fig. 20: Effect of manufacturing inaccuracies

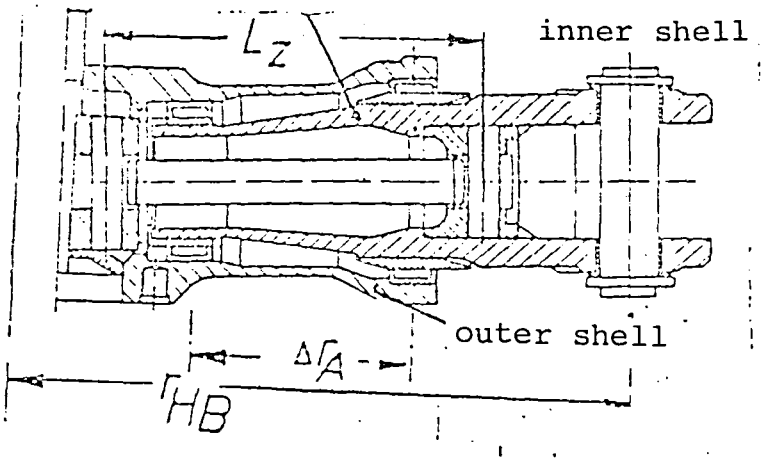

Fig. 21: Rotor head of a 4-blade rotor

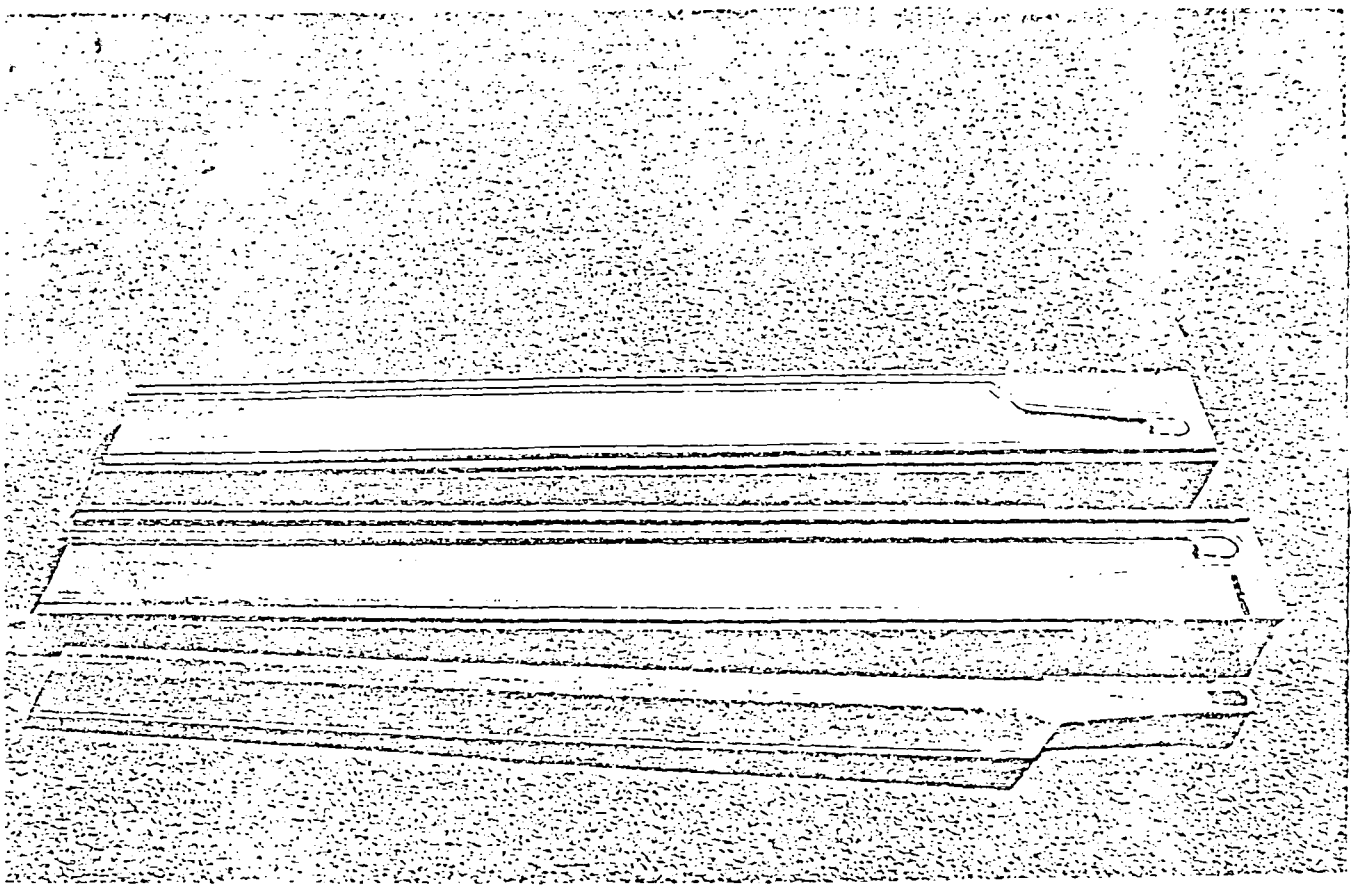

Negative mold for producing model rotor blades

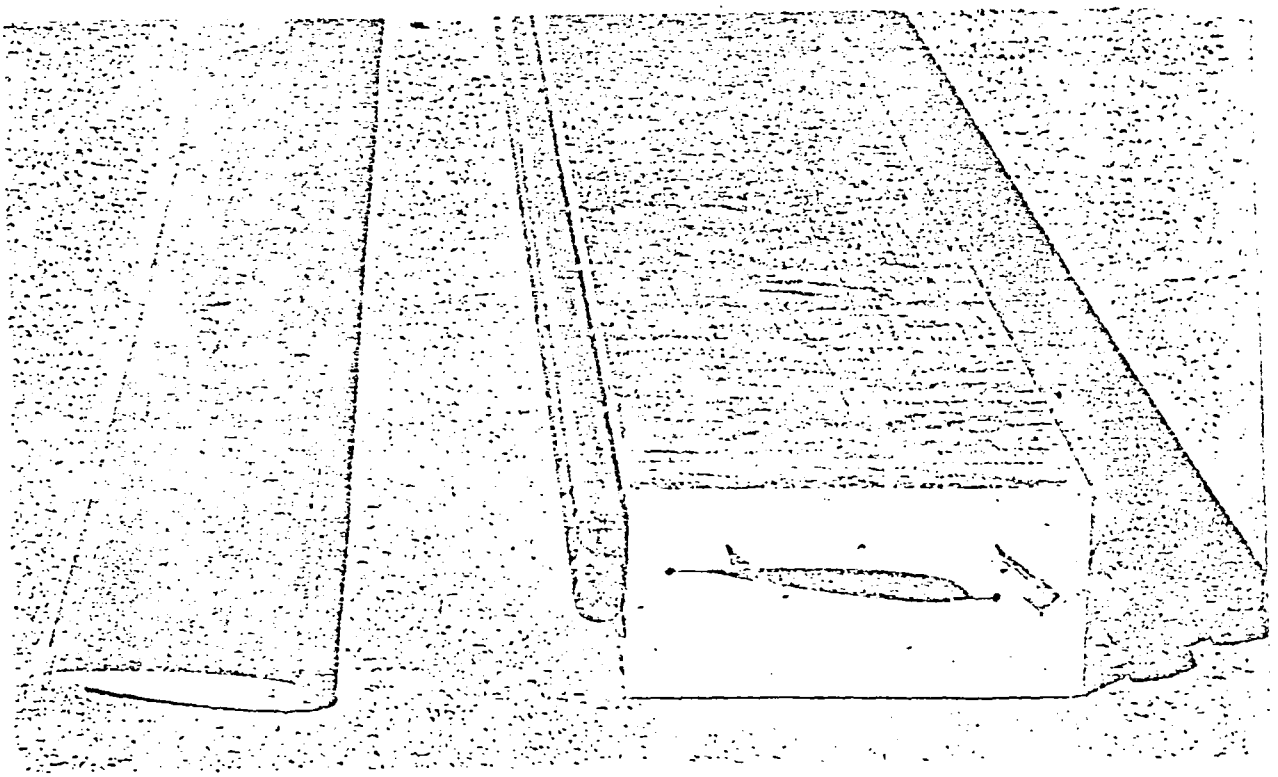

Blade profile NACA 23012 and negative mold

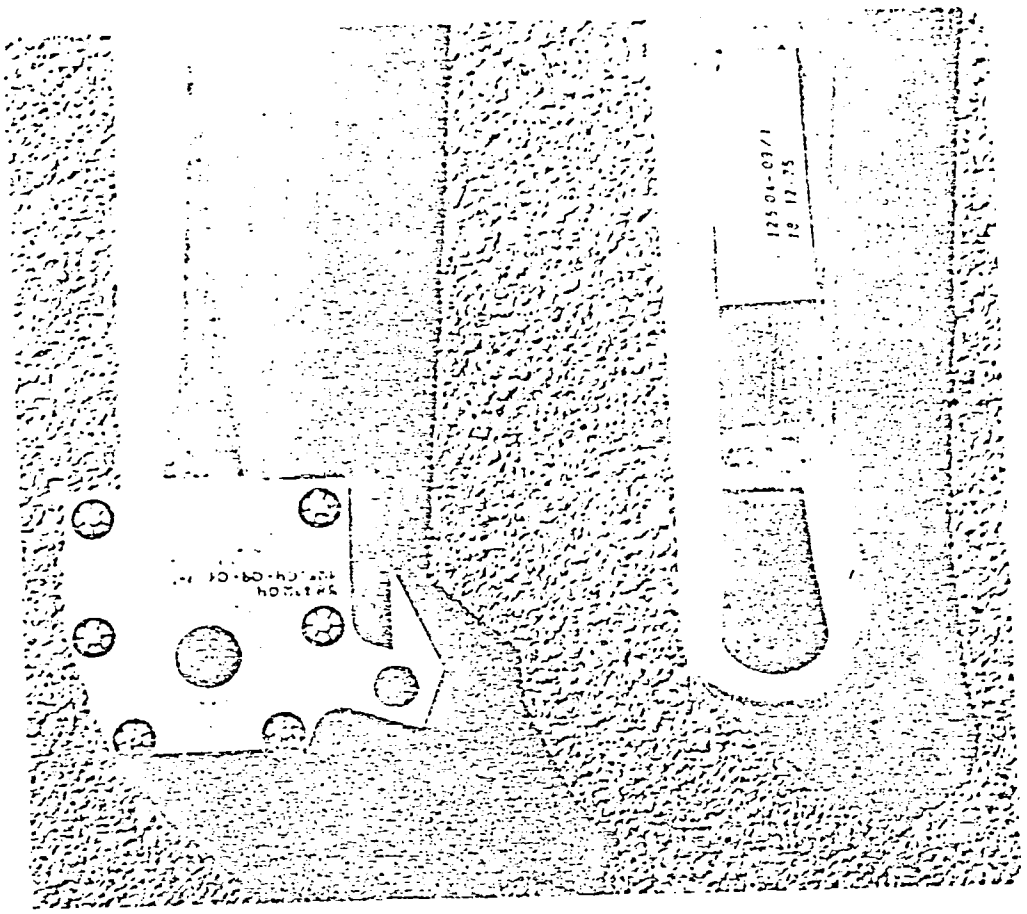

Fig. 23: Blade connection fitting and GFK cartridge embedded in it

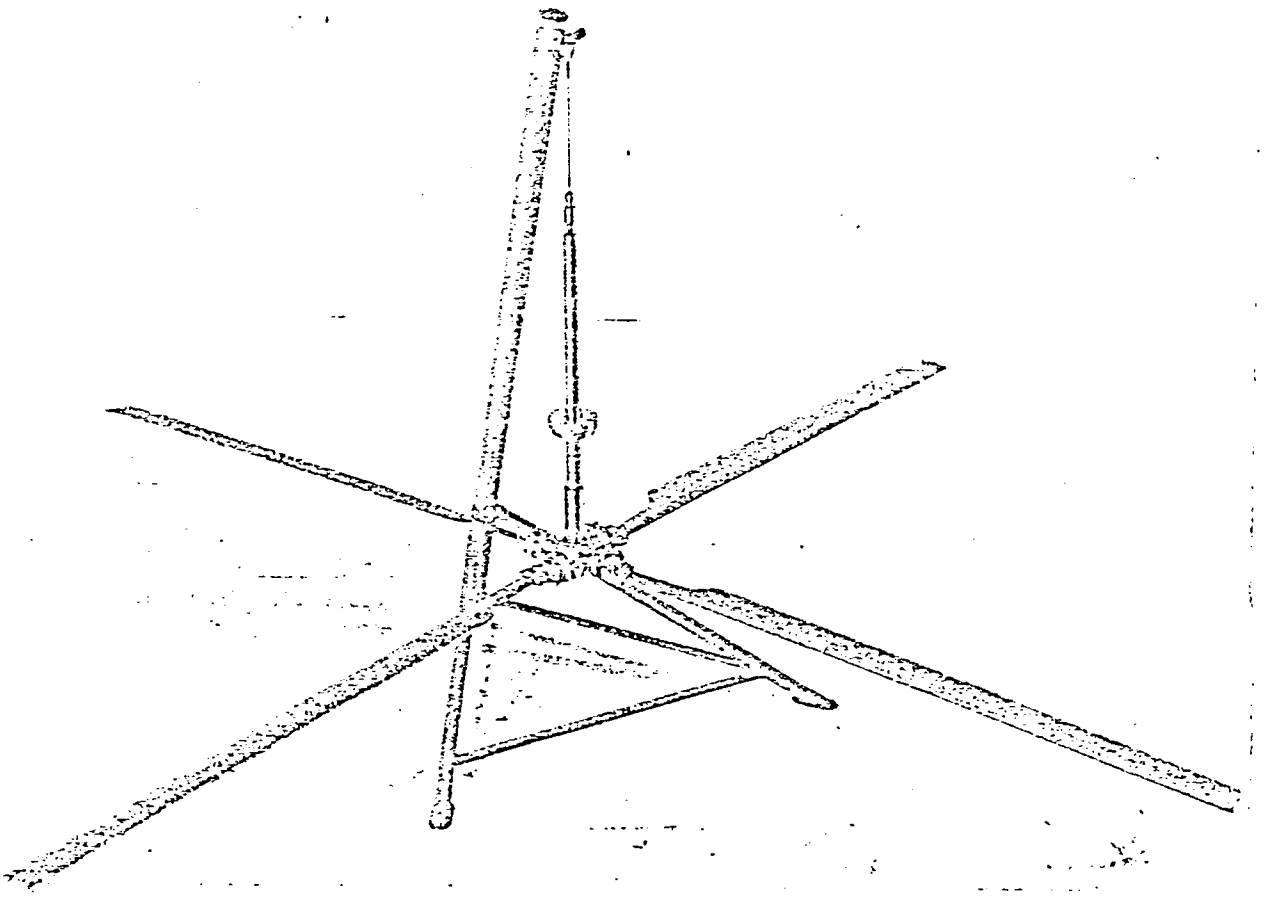

Fig. 24: Model rotor with static balancing on marvel device

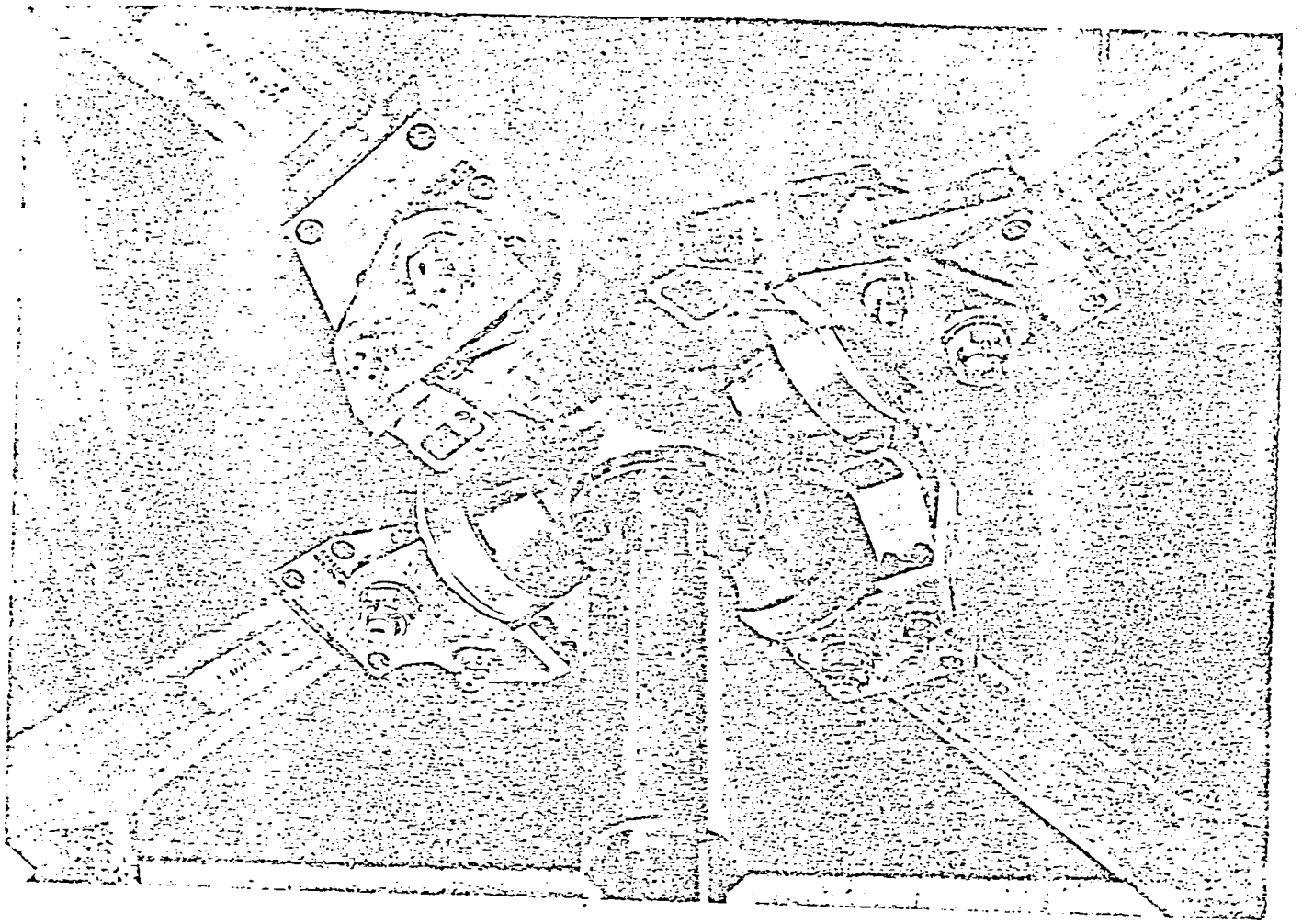

Fig. 25: Model rotor head installed

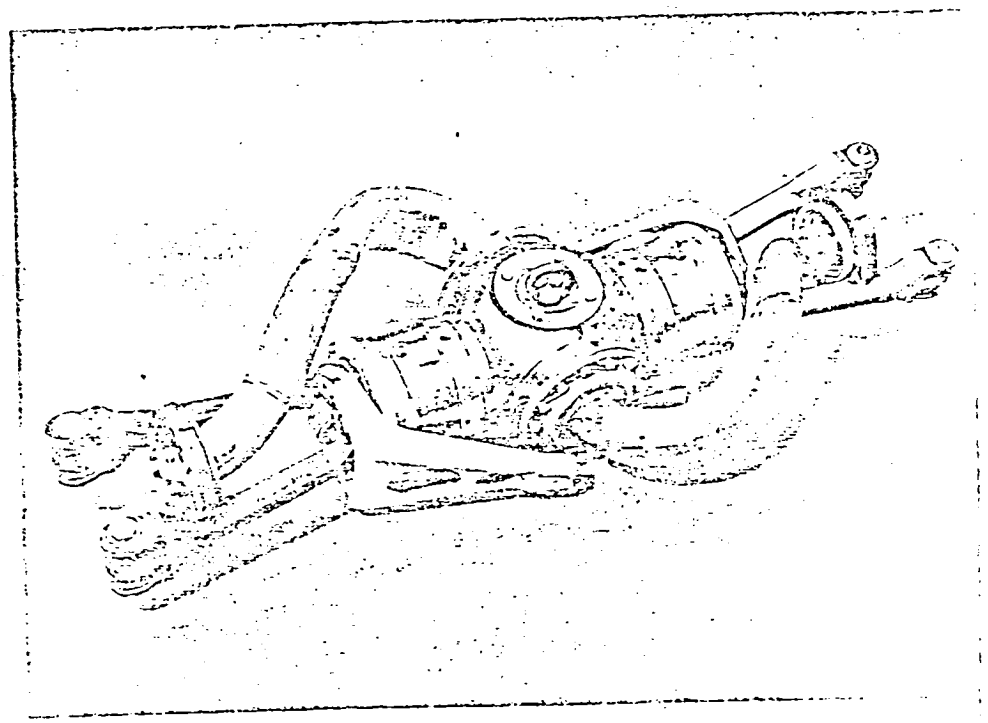

Rotor head

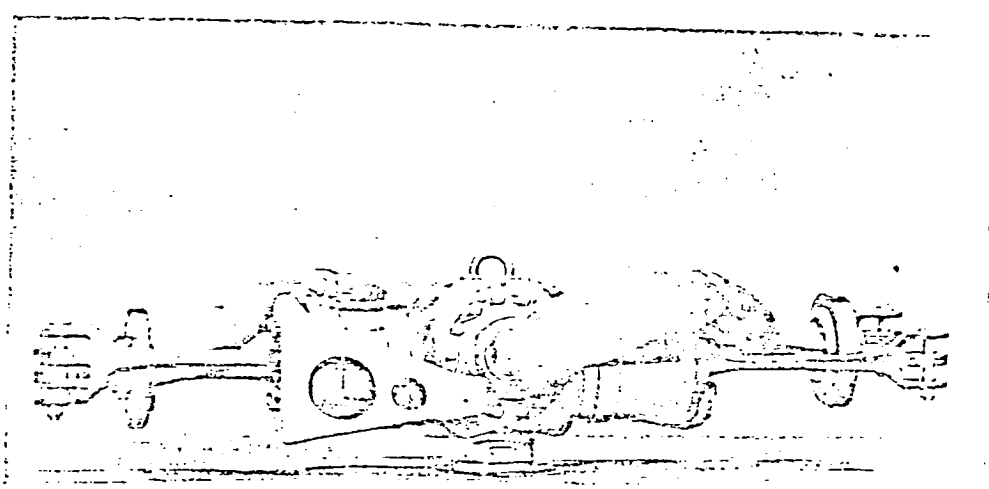

Fig. 26: 2-blade rotor with gas line

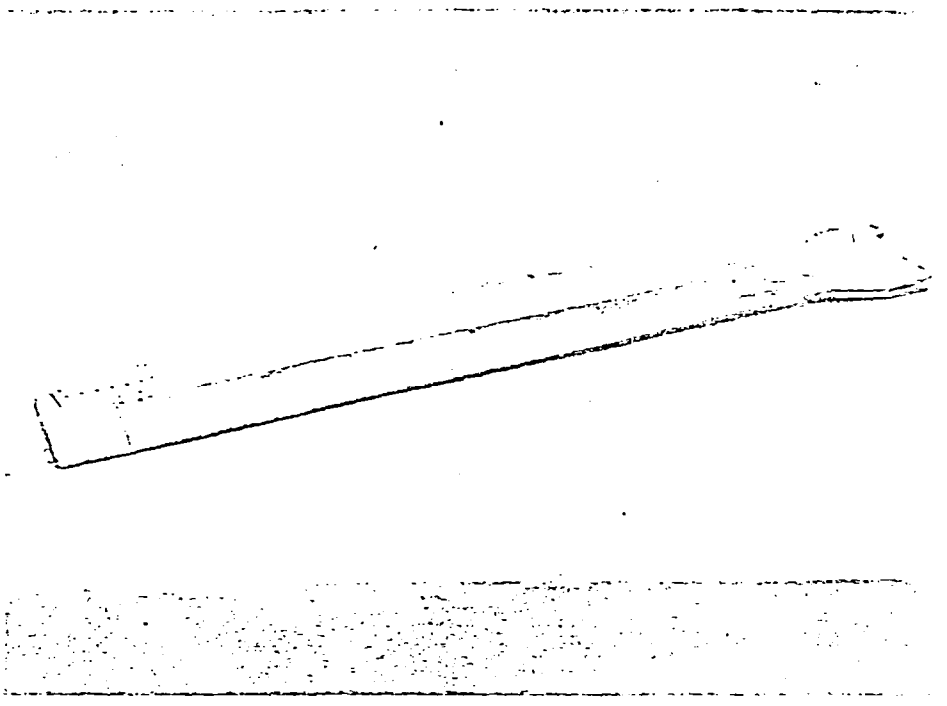

Fig. 27: Rotor blade of the 2-blade rotor

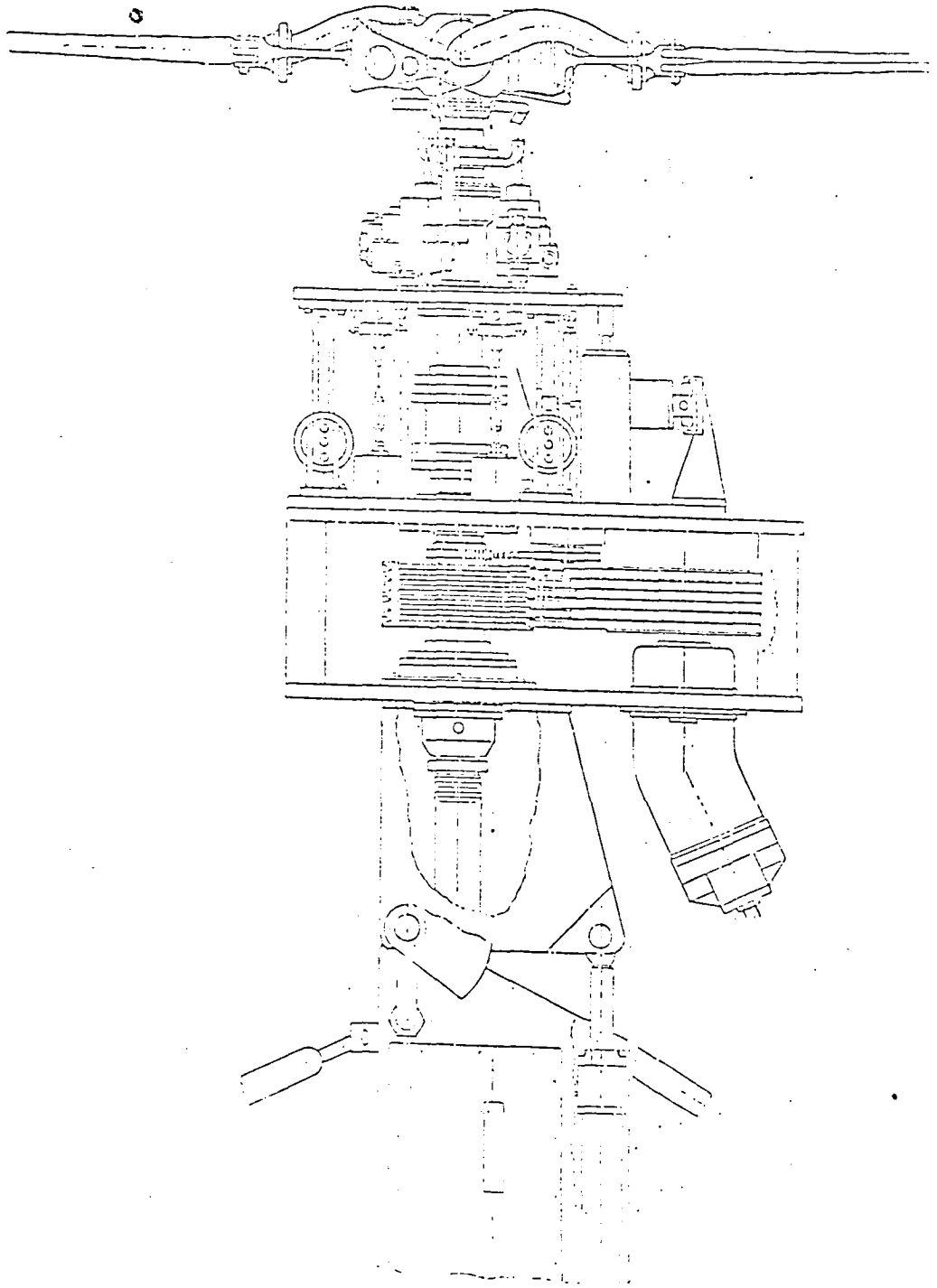

Fig. 28: Rotor test stand with hybrid drive (design structure)